AD-A086 996 NAVAL RESEARCH LAB WASHINGTON DC F/6 18/1
NRL RESEARCH IN SUPPORT OF THE DOE CHARGED-PARTICLE INERTIAL-CO--ETC(U)
JUN 80 D MOSHER, G COOPERSTEIN, S A GOLDSTEIN
UNCLASSIFIED NRL-MR-4237 SBIE-AD-E000 483 NL

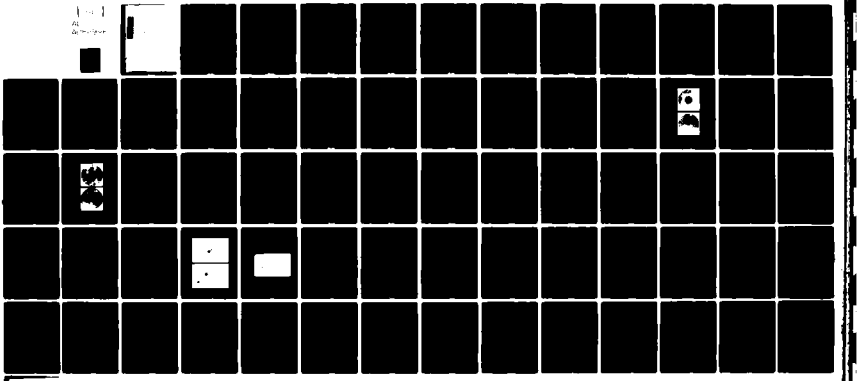

END
DATE FILMED
9-80
DTIC

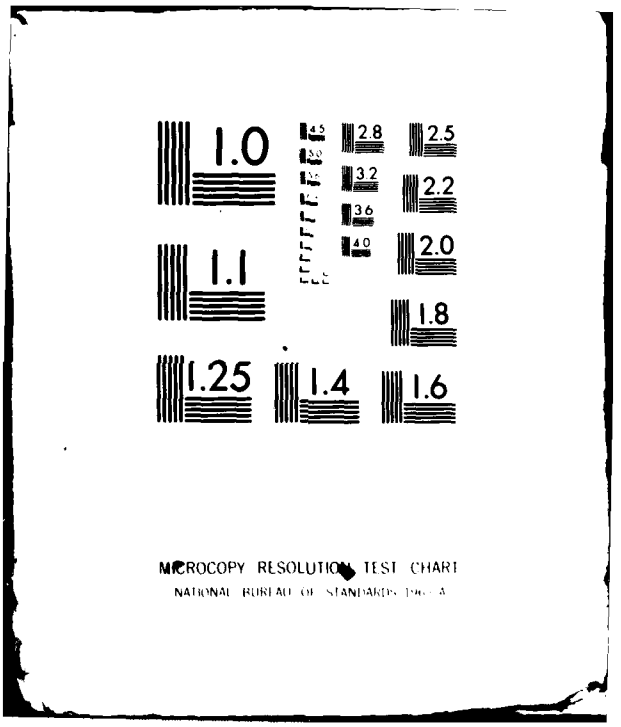
1.0
1.1
1.25
1.4
1.6
1.8
2.0
2.2
2.5
2.8
3.2
3.6
4.0
MICROCOPY RESOLUTION TEST CHART
NATIONAL BUREAU OF STANDARDS 1963-A

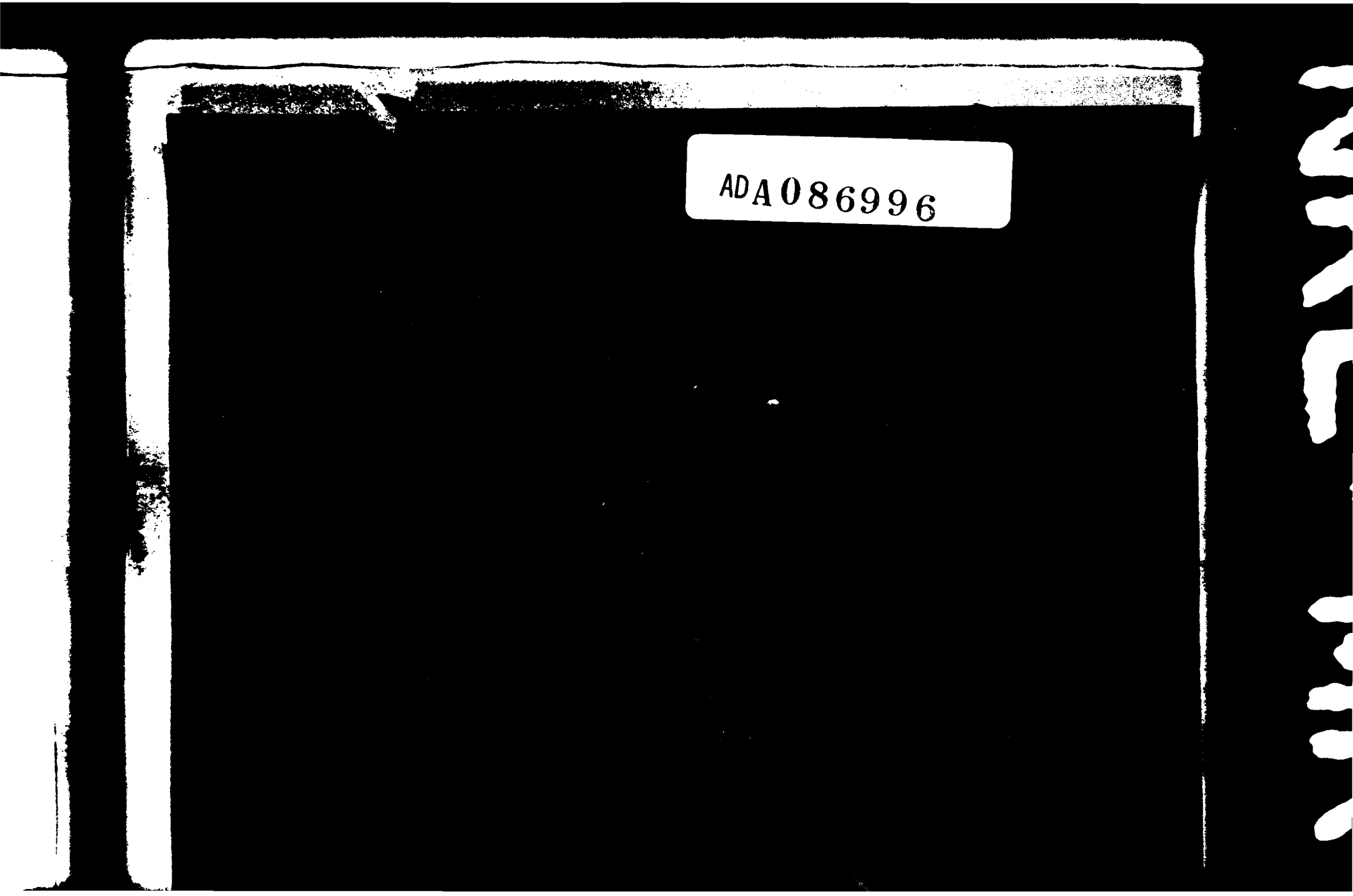

(14) NRL-MR-4237

SECURITY CLASSIFICATION OF THIS PAGE (When Data Entered)

REPORT DOCUMENTATION PAGE	READ INSTRUCTIONS BEFORE COMPLETING FORM
1. REPORT NUMBER: NRL Memorandum Report 4237	2. GOVT ACCESSION NO.: AD-A086 996
	3. RECIPIENT'S CATALOG NUMBER
4. TITLE (and Subtitle): FINAL REPORT OF NRL RESEARCH IN SUPPORT OF THE DOE CHARGED-PARTICLE INERTIAL-CONFINEMENT-FUSION PROGRAM FOR FY 77-78	5. TYPE OF REPORT & PERIOD COVERED: Final report
	6. PERFORMING ORG. REPORT NUMBER
7. AUTHOR(s): D. Mosher, G. Cooperstein, Shyke A. Goldstein[1], D. P. Bacon, D. G. Colombant, D. J. Johnson,[3] Roswell Lee,[4] W. F. Oliphant, P. F. Ottinger,[5] and F. Sandel[6]	8. CONTRACT OR GRANT NUMBER(s)
9. PERFORMING ORGANIZATION NAME AND ADDRESS: Naval Research Laboratory, Washington, D. C. 20375	10. PROGRAM ELEMENT, PROJECT, TASK AREA & WORK UNIT NUMBERS: NRL Problem 67-0879-0-0
11. CONTROLLING OFFICE NAME AND ADDRESS: Department of Energy, Washington, D. C. 20545	12. REPORT DATE: June 1980
	13. NUMBER OF PAGES: 67
14. MONITORING AGENCY NAME & ADDRESS(if different from Controlling Office)	15. SECURITY CLASS. (of this report): UNCLASSIFIED
	15a. DECLASSIFICATION/DOWNGRADING SCHEDULE

16. DISTRIBUTION STATEMENT (of this Report)

Approved for public release; distribution unlimited.

17. DISTRIBUTION STATEMENT (of the abstract entered in Block 20, if different from Report)

18. SUPPLEMENTARY NOTES

This research was supported by the Department of Energy Project No. 67-0879-0-0.

[1]JAYCOR, Alexandria, VA 22304
[2]JAYCOR, Alexandria, VA 22304
[3]SANDIA, Albuquerque, NM 87115
[4]JAYCOR, Alexandria, VA 22304
[5]JAYCOR, Alexandria, VA 22304
[6]JAYCOR, Alexandria, VA 22304

19. KEY WORDS (Continue on reverse side if necessary and identify by block number)

Light-ion beams
Inertial-confinement fusion
Proton and deuteron beams
Focusing
Transport

20. ABSTRACT (Continue on reverse side if necessary and identify by block number)

This report and publications referenced within document the NRL effort in support of the DOE charged-particle ICF program for the FY 77-78. Research in the areas of new charged-particle beam diodes and transport is reviewed.

DD FORM 1 JAN 73 1473 EDITION OF 1 NOV 65 IS OBSOLETE
S/N 0102-014-6601

SECURITY CLASSIFICATION OF THIS PAGE (When Data Entered)

251950

CONTENTS

FINAL REPORT OF NRL RESEARCH IN SUPPORT OF DOE CHARGED-PARTICLE INERTIAL-CONFINEMENT-FUSION PROGRAM FOR FY 77-78

I. INTRODUCTION TO THE RESEARCH PROGRAM

During the reporting period, Plasma Physics Division research has contributed to the Department of Energy charged-particle-beam inertial confinement fusion program in two major areas:

- electron-beam diode physics investigating the achievement of predictable and reproducible intensely-pinched beams
- charged-particle-beam transport physics for pellet-ignition systems employing electron, light-ion and heavy-ion beam drivers.

This report documents research in these areas which has not appeared in print in Sec. II-V. Published papers and reports which support the FY 77-78 DOE program are listed in Sec. VI and are referenced as subsection letter headings.

A. ELECTRON-BEAM DIODE RESEARCH

Electron-beam diode physics research carried out during the reporting period can be divided into two categories:

- Detailed experimental and theoretical investigations of the behavior of conventional tapered, pinched-electron-beam diodes.

Manuscript submitted April 29, 1980.

- Preliminary experimental and theoretical investigations of a novel diode configuration.

Research in the first category provides scaling relations for the electrical characteristics of diodes and documents electron-electrode interaction information required to achieve highly-focused beams. Work in the second category documents the behavior of a diode configuration with improved coupling characteristics to low-impedance generators and high current density capability.

Papers VI A-C cover the first category. The time-dependent impedance behavior of large-aspect-ratio pinched electron-beam diodes with no external magnetic field is investigated using the Gamble I and Gamble II generators in Sec. VI A. The experimental results are compared to predictions of a time-dependent computer code which incorporates several important mechanisms that affect diode impedance. A discussion of these mechanisms including experimental evidence of their existence and their effects on the observed diode impedance is presented. A simple model for the current is used in a time-dependent analysis of the data in order to demonstrate qualitative effects. The rise time of the electric field, the cathode-plasma velocity, the time-dependent generation of ion sources from the anode, and the special diode geometries (tapered cathodes) are shown to affect the diode impedance in good agreement with theory.

The effect of different anode materials on the size of very intense pinches is studied using the radial structure of the bremsstrahlung from a tightly pinched relativistic electron beam in Sec. VI B. Time-dependent data are obtained which point out the influence of scattering by the anode which electrons experience near the pinch axis. The scattering broadens the bremsstrahlung FWHM for pinches with high-Z (80) anodes to 6 mm, compared to 4 mm for

low-Z (13) anodes. When anodes composed of low- and high-Z elements in different annular regions are used, translation of backscattered electrons enhances the current density upon the low-Z regions and decreases it upon the high-Z regions.

In paper VI C, the EUV emission from 10- to 100-mg/cm^2-thick planar targets (Z = 6-79) exposed to 60-nsec duration focused relativistic electron beams was examined at current densities of 0.4 – 1.0 MA/cm^2. Spatially resolved spectra were obtained with a stigmatic near-normal incidence spectrograph, in the wavelength range 500-2100 Å, along axial radial directions. Time-resolved EUV data were obtained with windowless photoelectric diodes operated unfiltered and filtered with 0.5-μm-thick aluminum. The axial views show copious emission from the diode gap associated with late-time impedance collapse. Radial views show continuum radiation which is emitted from the region of the target exposed to the focused REB and line radiation which originates from a lower-density (approximately 10^{19} cm^{-3}) more-extended late-time plasma resulting from foil expansion. The region of the foil exposed to the focused REB radiates as a blackbody source with a peak temperature of 2-6 eV. These temperatures are a factor of 2 below the calculated temperatures for classical deposition in the foils exposed to the focused beam assuming no hydrodynamic foil expansion.

A radial-injection electron beam diode configuration is discussed in Sec. II. It combines a bias-current pinch and an ion-induced pinch. This technique allows one either to minimize the ion current or to concentrate it near the axis. The radial injection was attempted as a smooth transition for electrons from the cathode to equipotential surfaces. A comparison of analytic theory, numerical simulation results, and experiments indicates that bias-current pinching via paravector-potential (PVP) flow was realized without reduction of ion flow in the large area regions. Detailed geometries of diodes specifically designed to allow a smooth transition from a

PVP flow at large radii to an ion induced pinch flow at small radii were studied. Electron pinching from 110 mm to 3 mm was observed with corresponding three order of magnitude current density enhancement.

B. CHARGED-PARTICLE-BEAM TRANSPORT RESEARCH

During the reporting period, research for electron, light ion and heavy-ion beams was carried out in order to determine the feasibility of transporting focused or focusing beams through a pellet-fusion reactor chamber. The investigations carried out include:

- High-current electron beam transport experiments on the Gamble I and Gamble II generators.
- Theoretical investigations of focusing and transport of light-ion-beams in external magnetic fields.
- Experiments, theoretical and computational analyses of transport of light-ion-beams in channels, the MHD response of the channel, and microinstabilities of the beam-channel system.
- Theoretical assessment of heavy-ion-beam final transport with respect to beam neutralization and microinstabilities.
- Prediction of and estimates for enhancement in ion stopping power in ionized media.

In Section III, the propagation physics of hot electron beams in plasma discharges driven by exploding wires is described. This extended previous work carried out at Sandia Laboratories into a regime of higher beam currents (up to 300 kA injected) and investigated the effect

of channel current and diode voltage on beam propagation. The effects of scattering and axial electric fields on electron orbits as well as the limitations on the maximum beam current and beam current density that can be propagated was investigated. The experiment demonstrated that high-power-density electron beams may be efficiently transported using current-carrying air-plasma channels. It was shown that certain restrictions apply to their use, the most important being limitation of the current density. This restriction may be overcome to a certain extent by increasing the channel temperature. This might be accomplished by using a lighter background gas.

Research on transport and focusing of light-ion beams in external magnetic fields is summarized in Sections IV, VI D, and VI E. In the reflexive focusing scheme of Secs. IV and VI E, focusing on the pellet is achieved by employing a weak solenoidal field in the transport section, and introducing the beam at small angles to the field. The large gyro-radius motion of the ions then brings the beam to focus meters downstream. A drawback of this technique is that the location of the focus moves if the ion energy varies in time. Thus, time-of-flight bunching of the beam cannot be achieved.

In Section VI D, magnetic compression of a cold, charge-neutralized ion beam due to passage through a slowly varying magnetic-mirror field is studied. Conditions on the field and beam parameters are derived which permit the beam to be compressed to order-of-magnitude higher current densities while preserving the laminar nature of the flow. Effects associated with rotation, beam convergence, and velocity shear in the incident beam, and those due to self-fields are included in the analysis. It is shown that this approach is of limited value for focusing to pellet dimensions because of self-field effects and the need for an unrealisticly large applied field for a reactor scenario.

The channel transport technique used for electron beams is extended to light ion beams in Section VI E. By confining a beam already focused to pellet dimensions in an externally-driven discharge channel, delivery to the pellet can be accomplished with the time-varying ion energies appropriate for beam bunching. In Sec. V, MHD computations illustrate that an upper limit of about 1 MA of beam current exists because of plasma channel expansion. The expansion reduces magnetic confinement of the transporting beam causing radial beam expansion and loss. Calculation of growth rates for electrostatic instabilities in the beam-plasma system in Section VI F indicate that this class of instabilities does not inhibit transport for beams satisfying the MHD constraints.

Preliminary light-ion transport experiments are discussed in Sec. VI G. The discharge channel was established along a 50 cm thin wire embedded in a reduced air-pressure background. Although transport was demonstrated, the experiment was too crude to determine transport efficiencies. Additionally, the transported beam current was too low to assess difficulties associated with MHD response of the plasma channel or instabilities.

Plasma effects encountered by focusing heavy-ion beams traversing reactor-chamber backgrounds are summarized in Secs. VI H-J. Calculations of the degree of magnetic neutralization of the beam are treated in the first two entries. These calculations are important because even 1% non-neutralization may be sufficient to disrupt beam focusing on target for highly-stripped heavy-ion beams. Regimes for electrostatic microinstability of heavy ion beams are considered in Sec. VI J. As with light-ions, stability was found provided the beam parameters are consistent with currently-conceived reactor-level beams.

Finally, Sec. VI K provides an estimate of stopping-power enhancement expected for light and heavy ion beams due to ionization of the target material. About a factor-of-two enhancement is predicted for fusion-target temperatures.

II. PARAVECTOR-POTENTIAL DIODE RESEARCH

A. INTRODUCTION AND THEORY

Pinched electron flows in diodes have been used as a means of concentrating relativistic electron beam kinetic energy onto small areas. Inertial confinement fusion with relativistic electron beams has been a prime motivation for experimental and theoretical efforts directed at maximizing the electron power concentration. During recent studies, it was found that hollow cathodes generate a collapsing hollow ring[1] that pinches because of an ion-induced pinch.[2,3] Prior to these discoveries, it was speculated that the electron flow pinches in vacuum[4,5] due to the self-magnetic field generated by the electron flow current when it exceeded a critical current for pinching.[6] It has been shown that the relativistic effects[7] of unneutralized electron flows under self-magnetic fields do not generate a tightly pinched electron flow, but rather a weakly pinched one. The reason for this is that

$$|\mathbf{E}|_{\text{SELF}} > |\mathbf{B}|_{\text{SELF}} \tag{1}$$

and electrons do not $\mathbf{E} \times \mathbf{B}$ drift under such conditions. The models[4,5] for vacuum pinching, however, can be made self-consistent by adding a mysterious current flowing on the diode axis. This current adds to the total magnetic field reversing inequality (1). The resulting electron flow is described by a force-free flow which has been coined[4,5] Para-Potential Flow (PPF). One may then summarize the ion-induced pinch and the PPF described above for generating pinched electron flow as two ways of reversing inequality (1). The ion-induced pinch introduces ions that reduce the electric field while the PPF scheme introduced a bias current that increases the magnetic field. The latter shall be called a bias-current pinch since the PPF is only one of a family of electron flows that $\mathbf{E} \times \mathbf{B}$ drift towards the diode axis.

There is a definite advantage of bias-current pinches over ion-induced pinches for low impedance ($\leqslant 1\ \Omega$) generators. The ion current that flows in low impedance pinched-beam diodes restricts[2,8] the electron power to a finite level ($\sim 10^{12}$W) and is thus an unacceptable power drain for electron-beam fusion (but is an interesting source of power for ion beams[2,9]). Historically, there were many attempts to generate bias-current pinches. These included the use of (1) tapered hollow cathodes[10], (2) a plasma column on the diode axis,[11] (3) an externally-driven rod on the diode axis,[12] (4) two concentric cathodes,[13] and recently (5) multiple cathodes.[14]

Here, we report on a new technique that is a combination of a bias-current pinch and an ion-induced pinch (Fig. 1). This technique allows one either to minimize the ion current or to concentrate it near the axis. In addition, electron injection into the diode is radial rather than the axial emission of electrons from cathodes used to date. The radial injection was attempted as a smooth transition for electrons from the cathode to the equipotential surfaces (see the electron trajectories shown in Figure 1). Since electrons must cross equipotentials starting from the cathode (where the potential $\phi = 0$) on their way to motion along the equipotential surfaces near the anode, they can not be characterized by a PPF theory. A more general theory which is restricted only to cold electron flow[7] shows that the mechanical momentum of the electron fluid is related to the magnetic field by

$$\nabla \times \mathbf{P} = -\frac{e}{c}\mathbf{B} \tag{2}$$

Since $\mathbf{B} = \nabla \times \mathbf{A}$, and $\mathbf{A}$ is free to be defined with the addition of any $\nabla\chi$ one may realize

$$\mathbf{P} = -\frac{e}{c}\mathbf{A} \tag{3}$$

by choosing $\nabla\chi = 0$. Thus, the electron mechanical momentum vector lies along the vector potential. Hence the *Paravector-potential* (PVP) diode.

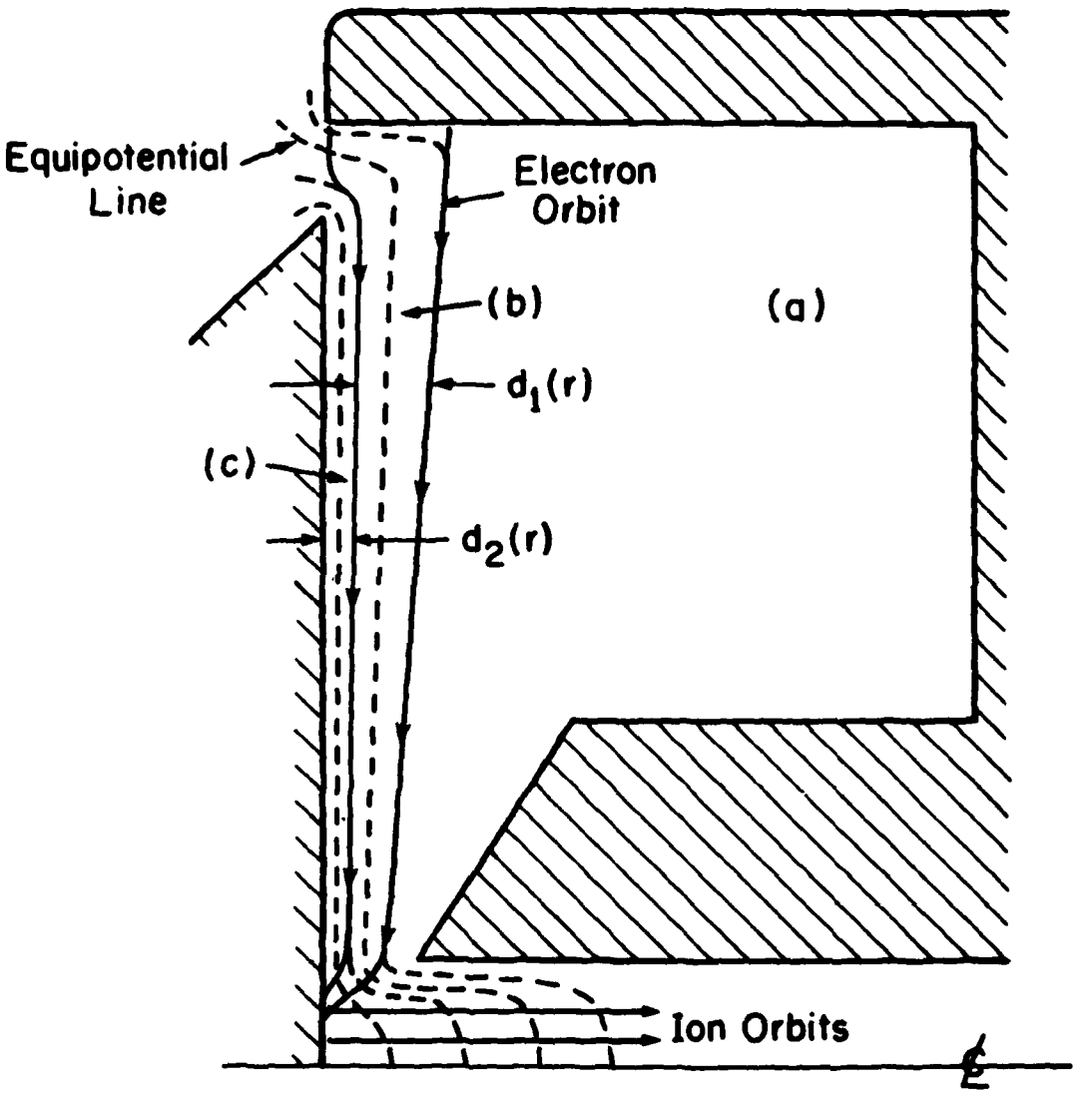

Figure 1 — A conceptual drawing of the PVP diode

The actual solutions of the electron flow for the geometry of Fig. 1 near the inner edge of the outer cathode and the anode edge are rather complicated. The exact solutions at smaller radii will depend on an analytic continuation of the flow pattern from the regions of the corners into the smooth region of the flat anode. A family of solutions which are exact solutions of the generalized equation[7] is given by a treatment similar to that of the reference.

The solutions are based on the existence of a region of zero electric field ((a) in Fig. 1), an electron sheath of thickness d_1 (region (b)), and a vacuum region of thickness d_2 (region (c)). The magnetic field in region (a) is derived from the bias current of the center cathode, and ions flowing to it from the anode. Electrons from the outer cathode flow without being lost on the anode at radii between two cathodes. Using the forms of the electric and magnetic fields of the electron flow as derived by Goldstein, et al.,[7] the thickness of the electron flow d_1, and the thickness of the flow-anode vacuum gap d_2 are found as functions of radius.

$$d_1 = r\left(\frac{I_o}{I_c}\right) F\left(\frac{I_t}{I_c}\right) \tag{4}$$

$$d_2 = r\left(\frac{I_o}{I_c}\right)\left(\gamma_o - \frac{I_t}{I_c}\right) G\left(\frac{I_t}{I_c}\right) \tag{5}$$

here r is the radius, $I_o = \dfrac{m_e c^3}{e} = 17$ kA, I_c is the center current, $\gamma_o = 1 + \left|\dfrac{eV_o}{m_e c^2}\right|$, V_o the diode voltage, and the functions F and G are given by

$$F(x) = 1/2 ln\ [x + (x^2 - 1)^{1/2}] \tag{6}$$

$$G(x) = 1/2\left[\frac{x + (x^2 - 1)^{1/2}}{x^2 + x(x^2 - 1)^{1/2} - 1}\right]. \tag{7}$$

Over the range $2 \leqslant x \leqslant 3$, $F(x)$ and $G(x)$ are approximately 0.8 and 0.25, respectively. It is important to note that for a given diode voltage, the gaps are totally defined by the ratio $\dfrac{I_t}{I_c}$. The anode-cathode spacing in region (a) does not enter into the result.

Since d_2 must be positive (or else the electrons will strike the anode), I_c must be greater than $\frac{1}{\gamma_o} I_t$. As d_2 is the distance between the flow and the anode, it provides a measure of the axial anode perturbations that the diode can tolerate. For example, for diode parameters of 1 MV, 1 MA, and $\frac{I_t}{I_c} = 2.4$, the quantity $d_2 = .006r$ while d_1 is a factor of 5 greater. Thus, at a radius of 4 cm, one can tolerate anode imperfections on the order of 0.02 cm.

If only electron flow existed, then the space charge effect of the flow from the outer cathode as it came opposite the inner cathode would have decreased the electron flow from the inner cathode, thus decreasing the bias current, resulting in the loss of the electrons on to the anode opposite the inner cathode. Taking into account that an anode plasma is being produced opposite the inner cathode by the electron beam heating of the anode surface, it is seen that ion flow may provide space-charge neutralization negating the effect of the radial electron flow and replacing the partially-suppressed electron current. The sum of the electron and ion currents in the center cathode represents the needed bias current. The presence of the ion flow allows an ion-induced pinch to continue the pinching of the electron flow to radii smaller than the inner cathode. Numerical simulation[15,16] has shown that in this region, the drifts of electrons (such as the ∇B drift) are a prime cause for finite pinch radius. The use of smaller-hole cathodes is known[17] to generate smaller pinches and was also tried in experiments reported on here.

In the numerical simulation studies, an extension of the $r - z$ semistatic, particle-in-cell code was used to find the self-consistent, numerical solutions of electron and ion flows. In Fig. 2, the diode geometry and vacuum equipotentials are shown for diode parameters close to those used in the experiments. When self-consistent particle flows are generated in this diode, the equipotential field lines (Fig. 3) are drastically altered and shifted toward the anode in close

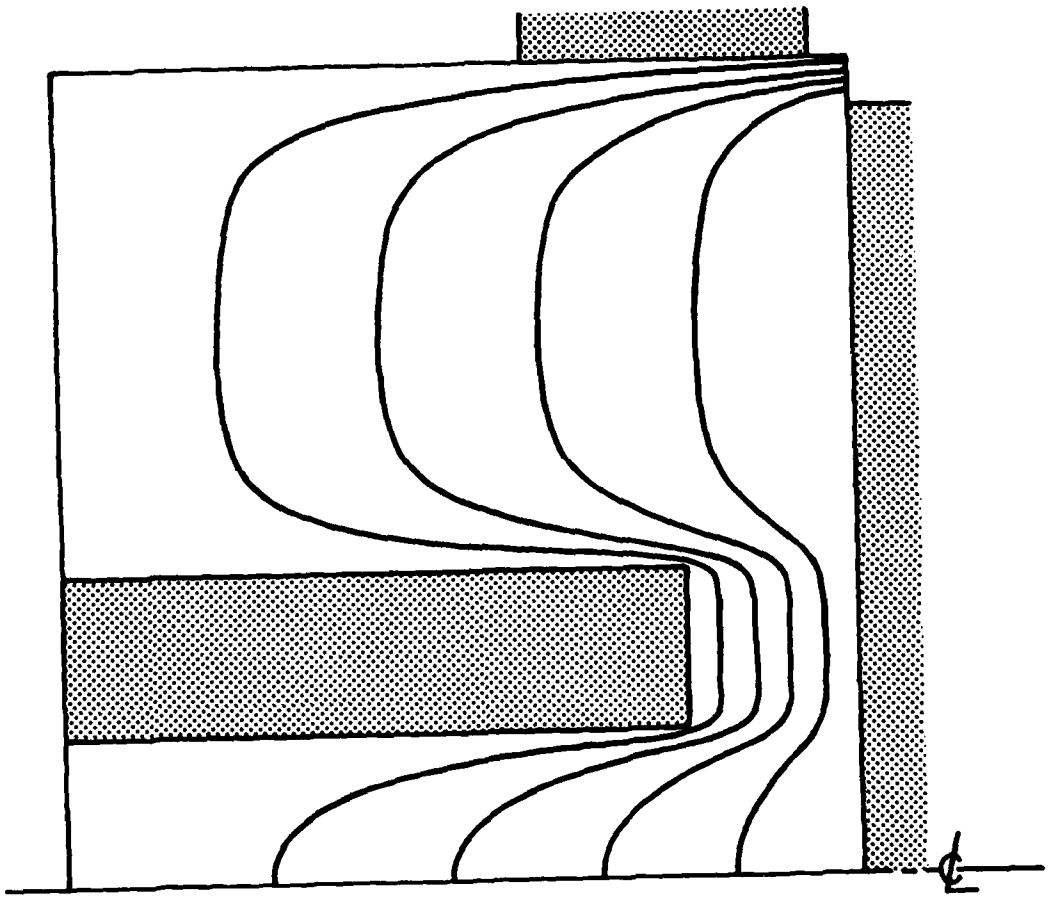

Figure 2 — Numerical simulation of equipotential field lines prior to electron emission

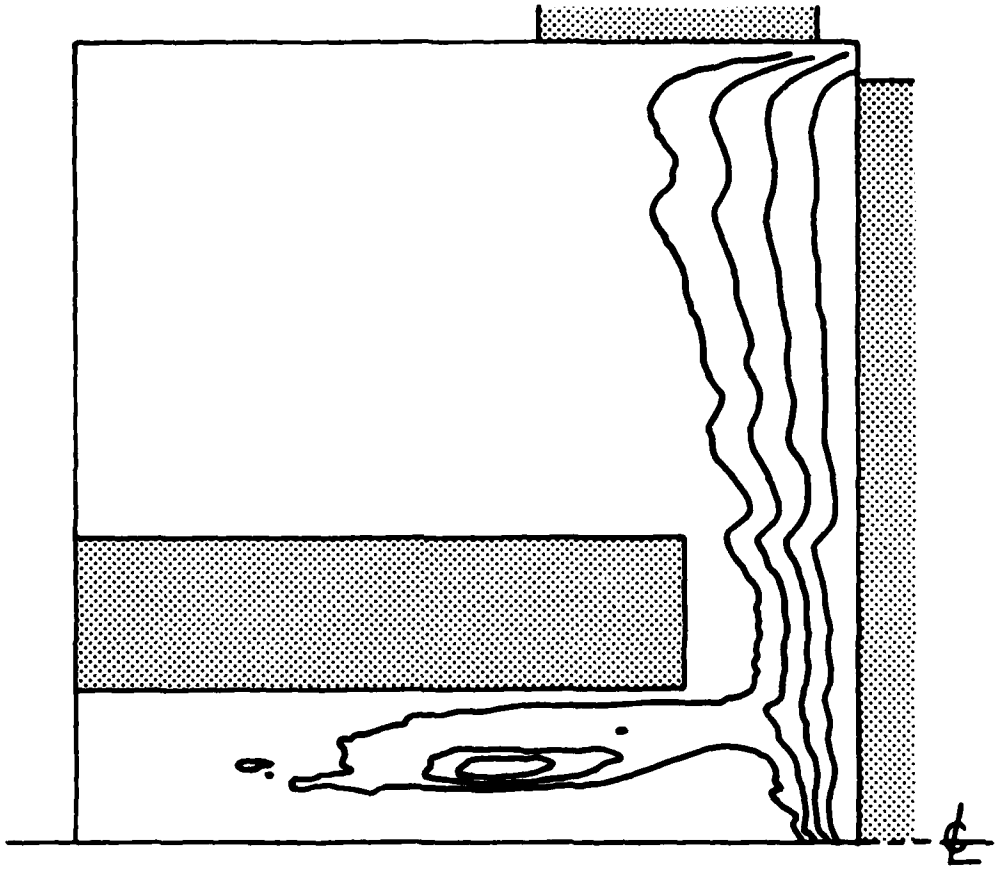

Figure 3 — Numerical simulation of equipotential field lines after 25 ns of electron emission

agreement with analytic theory. The only constraint imposed was that ions on the anode were generated at radii smaller than that of the inner cathode.

The basic concept of the PVP diode led to the design of a series of diodes used in conjunction with the GAMBLE I and GAMBLE II generators operated in positive polarity. The diode performance was studied over wide variations of voltage and total-to-center current ratio I_t/I_c. In agreement with theory, it was found that given a total-to-inner current ratio less than γ_o, the radially-injected electrons will flow inward without striking the anode at large radii providing there are no gaps or projections to perturb the equipotential surfaces. If the needed bias current is not provided, then a self-correcting phenomenon was observed in which excess radially-injected electrons are lost immediately to the anode edge. The rest flow in without striking the anode at large radii resulting in a current of $\gamma_o I_c$ near the anode axis. The other predicted phenomenon observed was the interaction of the radial electron flow with the bias flow. Instead of continually rising during the voltage pulse, the bias current clamped at the value it had at the time the radial flow started.

B. EXPERIMENTAL APPARATUS

The PVP diode design has worked over the course of more than 80 shots. A scale drawing of the latest geometry is shown in Fig. 4. The cathodes (shown solid) were made from brass and mounted on a 36 cm diameter, 2.5 cm thick aluminum insert (shown cross-hatched) which fit the doors of both of the GAMBLE relativistic beam generators when operated in positive polarity. The door insert has a 4.4 cm diameter hole on axis (originally 2.5 cm) and a 1.0 cm slit 22.9 cm long cut through it (originally 19.7 cm) for viewing a diameter of the anode. The taper of the inner cathode was varied from 6° to 30° with a variety of inner and outer diameters. The most recent inner cathode was the 8.2/1.3 cm (O.D./I.D.), 12° tapered hollow

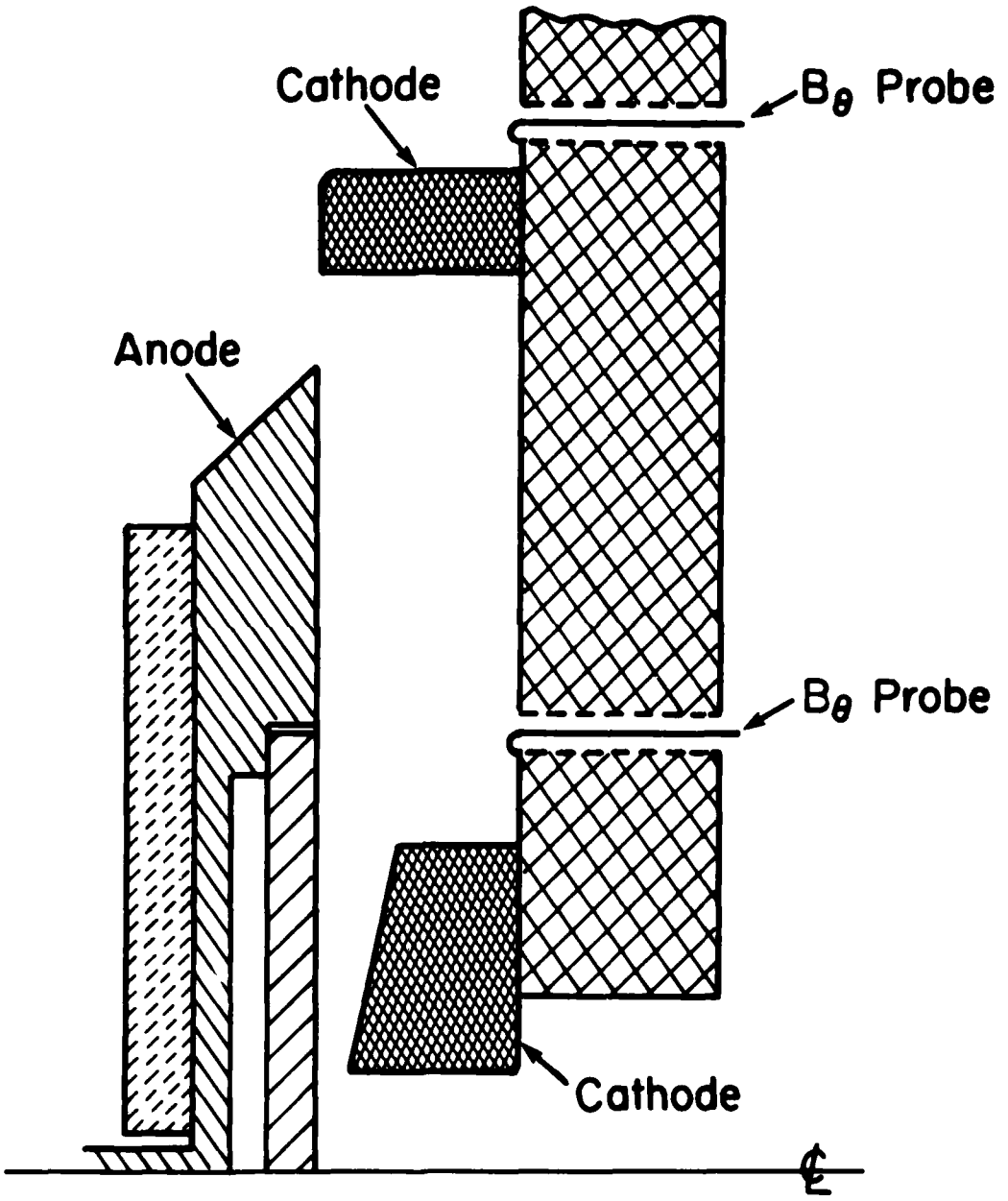

Figure 4 — Scale drawing of latest PVP diode

cathode shown in Fig. 4. The outer cathode was a 22.9 cm I.D., 25.4 O.D. brass ring. Shots using annular brass inserts to close the radial gap or tailor the emission surface have been taken. The anodes were originally flat aluminum disks (Fig. 5a) 20 cm in diameter which were held onto the center conductor of GAMBLE I or GAMBLE II by 6 insulating bolts at a large radius. On later shots, the anode diameter was increased to close the radial gap. Spacers allowed the anodes to be positioned so as to be in the plane of the outer cathode. Later, in an attempt to reduce the edge damage, the outer edge was beveled at 45° (Fig. 5b) to give the non-radially emitted electrons more distance in which to turn. Only in the last series of shots was the outer edge geometry changed to that shown in Figs. 4 and 5c — the anode edge being relatively sharp and the anode beveled at negative 45°. In this configuration, the axial electric field was reduced with the result that most of the current flowed radially. The anode was a 20.3 cm diameter, stainless steel outer structure (shown with fine hatching) which held an aluminum insert (shown with large hatching). The space behind the insert was present to prevent shock damage to the stainless holder and the hub of the generator. The stainless holder was mounted with a single 1/4" — 20 screw into the generator. The entire anode surface was covered with either 2 μm aluminized KIMFOL a polycarbonate foil or 6 μm aluminized mylar, aluminum side towards the cathode. The covering provided the anode with a smooth, continuous potential surface.

The main diagnostics were a diode voltage monitor, B loops monitoring the current flowing from the center cathode and from the total cathode assembly, anode witness-place damage, and x-ray production monitored by a time-integrated x-ray pinhole camera and calibrated p-i-n diodes.

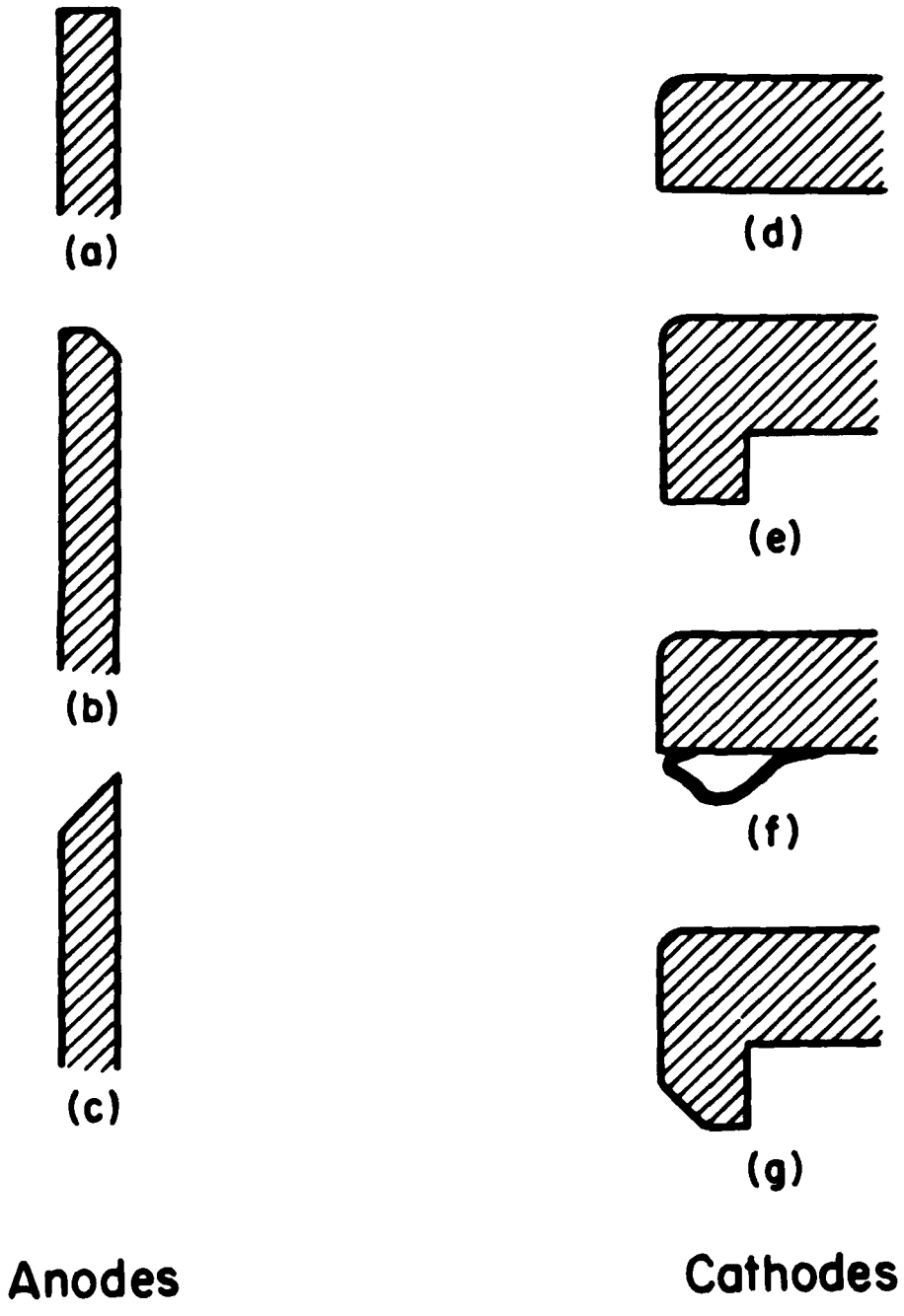

Figure 5 — Anode and outer cathode geometries used in these experiments

C. OBSERVATIONS

Series I — GAMBLE I Shots # 5828-5836

This series of shots used 20.0 cm diameter flat aluminum anodes mounted with six bolts at a diameter of 18.4 cm. The bolts were counterbored so as not to protrude out of the plane of the anode. An insert into the outer cathode made the radial gap 5 mm (see Fig. 5e). The anode was varied from being inserted 0.5 mm into the plane of the outer cathode to being withdrawn 0.5 mm from it. The inner cathode was an 8.4/3.9 cm (O.D/I.D.), 6° tapered hollow cathode and the anode-cathode gap was 5.2 mm at the inner diameter.

The voltage on these shots was low ($\lesssim$ 400 kV) and the bias current criterion was not met. Only 100 kA out of the 235 kA total current flowed in the center cathode which, according to the theory of PVP flow, could bring in 80 kA from the outer cathode leaving 55 kA to strike the anode rim. Anode rims showed existence of radial flow through their extensive damage. The inner edges of the screw holes showed evidence that the beam had struck them on its way in lending support for the existence of radial flow.

The other conclusion from this series of experiments is that the very large area anode (314 cm^2) could not turn on an anode plasma during the 50 ns pulse time so that an ion induced pinch could not take place. This is in agreement with the axial velocity[3] on aluminum ($\sim$ 2 cm^2/ns/100kA) which brought the collapsing hollow ring from a radius of 10 cm to a radius of 9 cm.

Series II — GAMBLE I Shots # 5837 and 5845

For these shots, the same aluminum anodes were used as well as the same inner cathode. However, the outer cathode had finger stock mounted on its inner edge instead of an insert (see Fig. 5f). The inner cathode provided the required bias current and was nearly equal to $\frac{1}{\gamma_o} I_i$ for almost the total pulse time. The anodes showed little edge damage and had a rear-surface spall of 1.1 cm diameter on axis. The x-ray pinhole photograph for shot #5845 shows a 7 mm (FWHM) pinch. Figure 6 shows the front (left) and back of the anode for shot #5845. Note the slight damage at the inner edge of the screw holes. Figures 7 and 8 show the diode parameters for the same shot. It is significant to note that the outer cathode did not turn on for 10-20 ns after the start of the current pulse. When the outer cathode did turn on, the inner cathode current was clamped at its then current value remained nearly equal to $\frac{1}{\gamma_o} I_i$ for the rest of the pulse. The value at which the inner current clamped was a factor of two below its operating value when used without the outer cathode. This agrees with our theoretical expectations of the effect of the radial electron flow on the behavior of the inner cathode.

Series III – GAMBLE I Shots #5847-5851

These shots were identical to the shots in Series II with the addition of a TRW streak camera looking at the ions emitted from the anode. The ions struck the silvered side of an optically-thin slab of Pilot-B scintillator covering a diameter. The scintillator was viewed with the streak camera. The streak camera photographs showed that there were no ions emitted at large radii (compared to the outer radius of the inner cathode) although there were some ions coming from just outside the inner cathode.

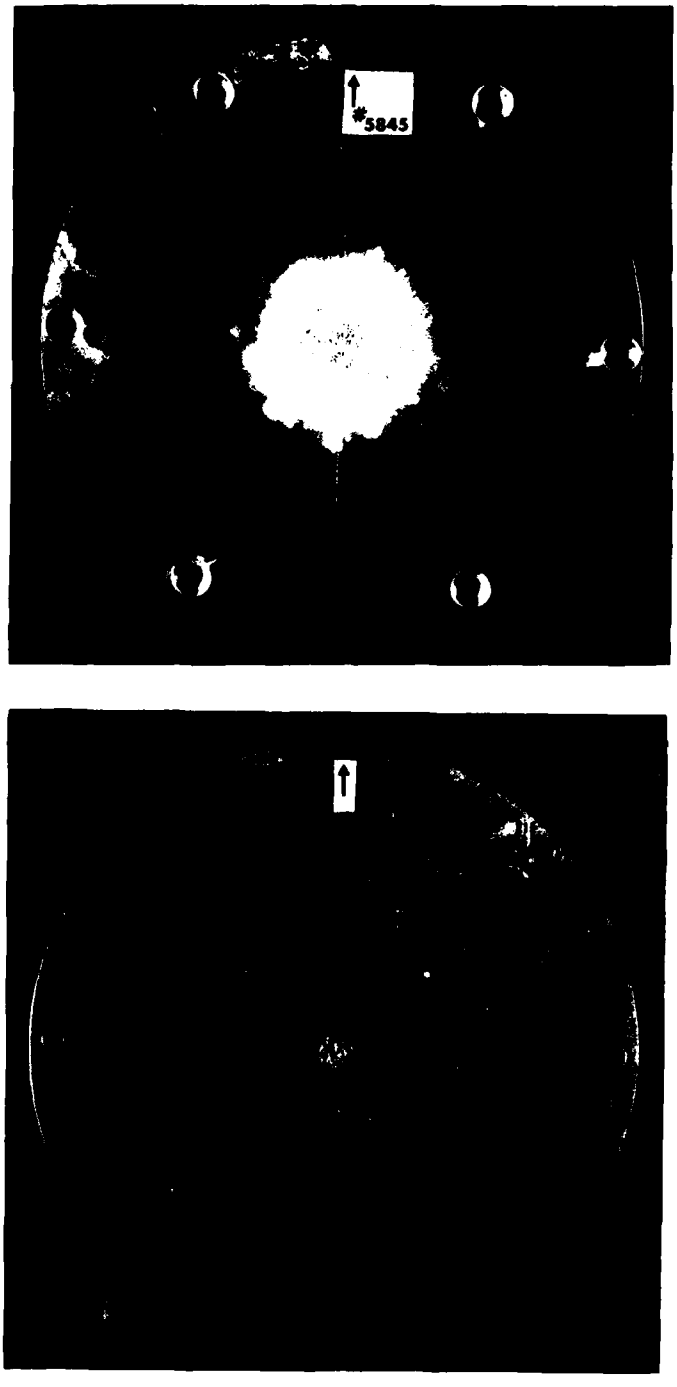

Figure 6 — Aluminum anode for shot #5845

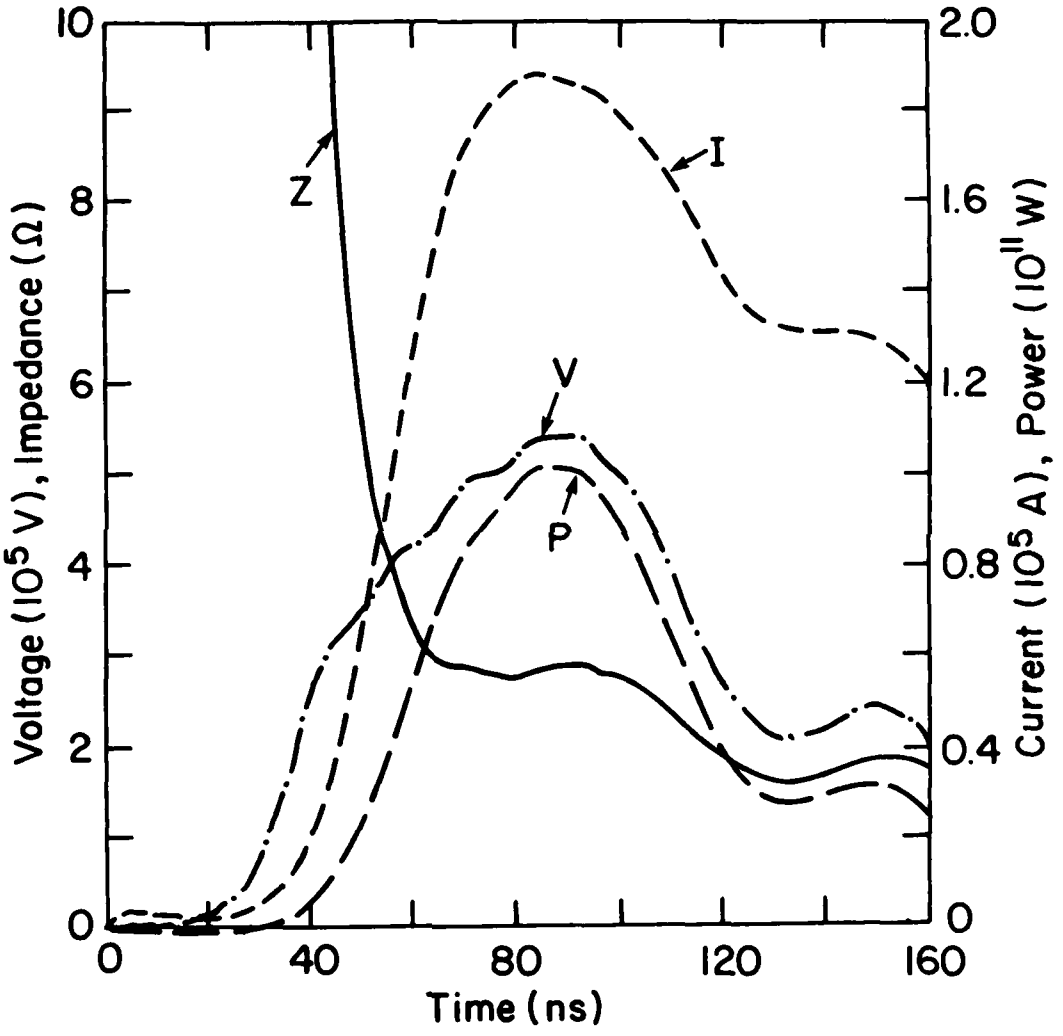

Figure 7 — Overall diode parameters for shot #5845

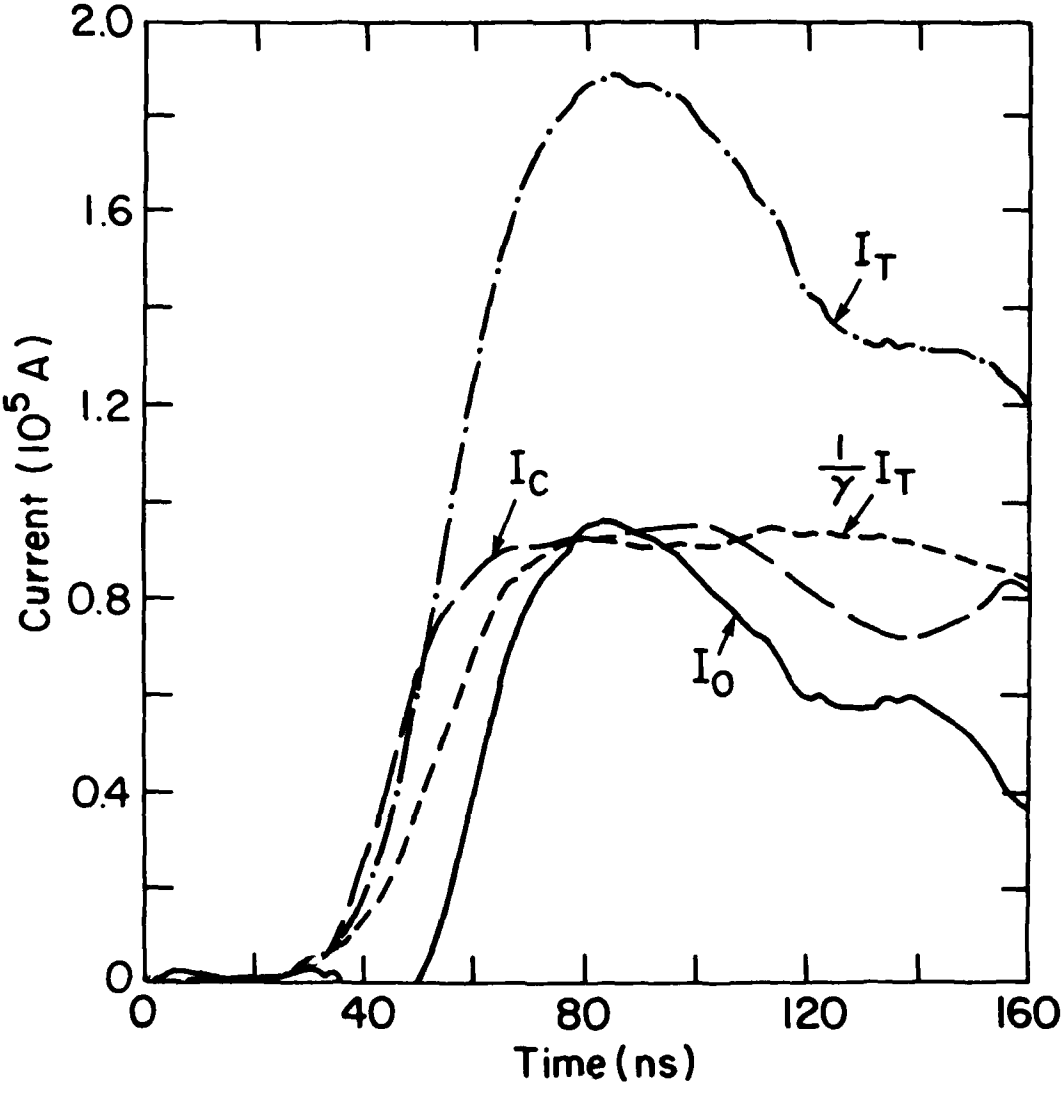

Figure 8 – Inner, outer, total, and theoretical bias current for shot #5845

Series IV — GAMBLE I Shots # 5861-5868

These shots had a 45° beveled outer cathode insert (Fig. 5g) and a 20.3 cm or 20.6 cm diameter, 45° beveled anode (Fig. 5c). The reduced radial gap meant that the voltage was again low and the required bias current not supplied. This geometry did not prove successful.

Series V — GAMBLE II Shots #1731-1735

For the first series of shots on the higher power GAMBLE II generator, 20.6 cm diameter, 45° beveled anodes (Fig. 5c) and an outer cathode with finger stock mounted on its inner edge (Fig. 5f) were used. On none of these shots was the $\frac{1}{\gamma_o} I_i$ bias current supplied. Nevertheless, shot #1735 appeared to be a relative success.

Figures 9 and 10 show the diode parameter for shot 1735. The diode operated at 750 kV, 900 kA with a flat, 0.5 Ω impedance during the plateau of the voltage pulse. Two things should be noticed. The bias current required to vacuum pinch (350 kA) all of the outer current was never supplied and there was no delay time between the start of the inner and outer currents. Even so, 400 kA out of a outer current of 650 kA should have vacuum pinched.

Figure 11 shows the front (left) and back of the anode plate for shot #1735. Although there was a great deal of damage to the anode edge due to the 250 kA of excess current, most of the anode outside of the inner cathode radius is relatively undamaged. Most of the apparent damage seen in Fig. 11 is aluminum melted by the pinch and deposited on the anode surface. The x-ray pinhole photograph confirms this as it shows relatively little x-radiation coming from the region between the anode edge and the inner cathode compared to radiation from the anode edge. This provides additional support for our theoretical expectation that $\gamma_o I_c$ will pinch with the excess outer current sloughing off to the anode edge.

Figure 9 — Aluminum anode for shot #1735

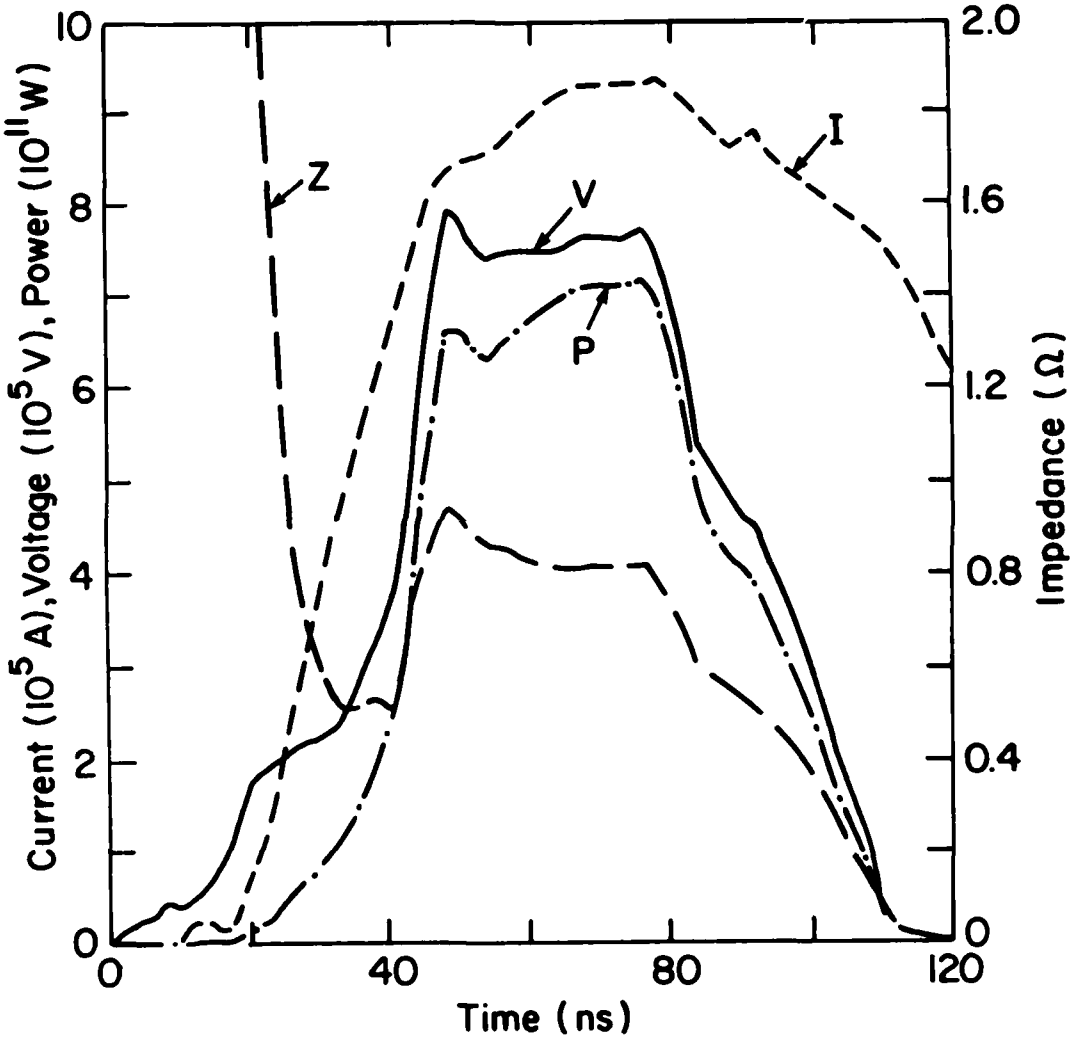

Figure 10 — Overall diode parameters for shot #1735

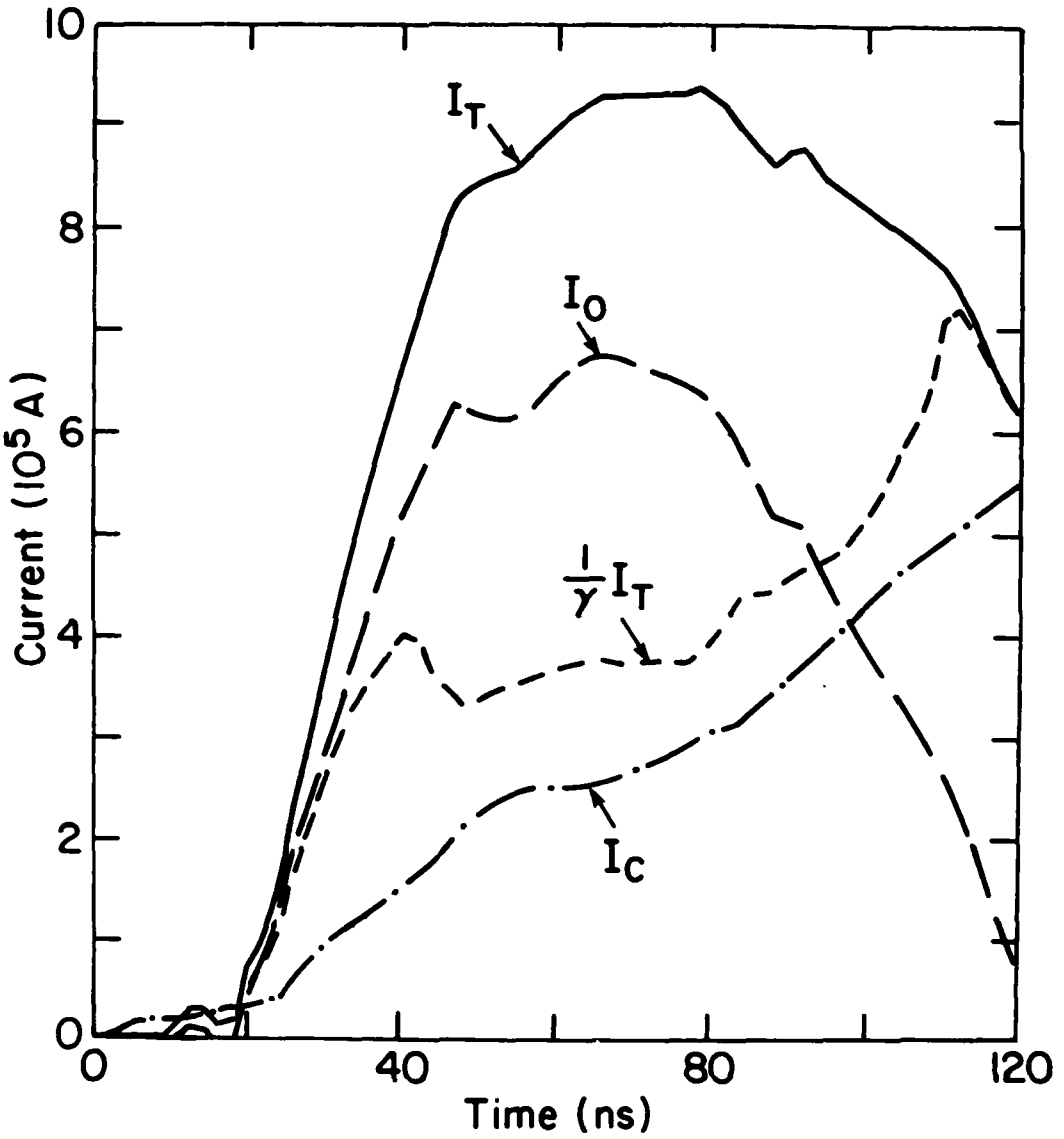

Figure 11 — Inner, Outer, Total, and Theoretical Bias Currents for shot #1735

Series VI — GAMBLE II Shots #1745-1748

These shots were identical to the last series except that the outer cathode had no finger stock insert (Fig. 5d) in order to open the radial gap, and the inner cathode was a 2.5 cm I.D., 2.9 cm O.D., 30° tapered, hollow cathode. The sharp-edged center cathode tended to either not supply very much current, or to short out. However, for shot #1748, the biasing criteria was satisfied through the peak of the voltage pulse (1 MV) but was not satisfied during the voltage fall. Again, the x-ray photograph shows little radiation between the anode edge and the inner cathode.

Series VII — GAMBLE I Shots # 6431-6447

This last series of shots used the geometry shown in Fig. 4, the design of which was based on considerations described earlier. The electrical characteristics and x-ray photographs showed that this new geometry almost always met the biasing criterion and that there were few or no x-rays from the anode edge. Also, this diode operated with a shot-to-shot reproducibility of 10% in current and voltage. Figures 12 and 13 are the averaged diode behavior for the five shots 6442-6446. As was typical of the earlier successful GAMBLE I shots, there is a 10-20 ns time delay between the start of the total current and the start of the outer current.

In order to study the ion current, the anode was modified by drilling a 1.3 cm diameter hole on axis and mounting a 2 cm diameter disk of 127 μm polyethylene over the hole. The anode was recessed slightly over the central 2 cm so that the polyethylene disk would not protrude. The mylar anode covering was cut away to expose this disk. The result of activation measurements on this system indicates that ion current densities of approximately 4 kA/cm^2 flow in the 2.5 cm diameter hole of the center cathode. These preliminary results will be further investigated.

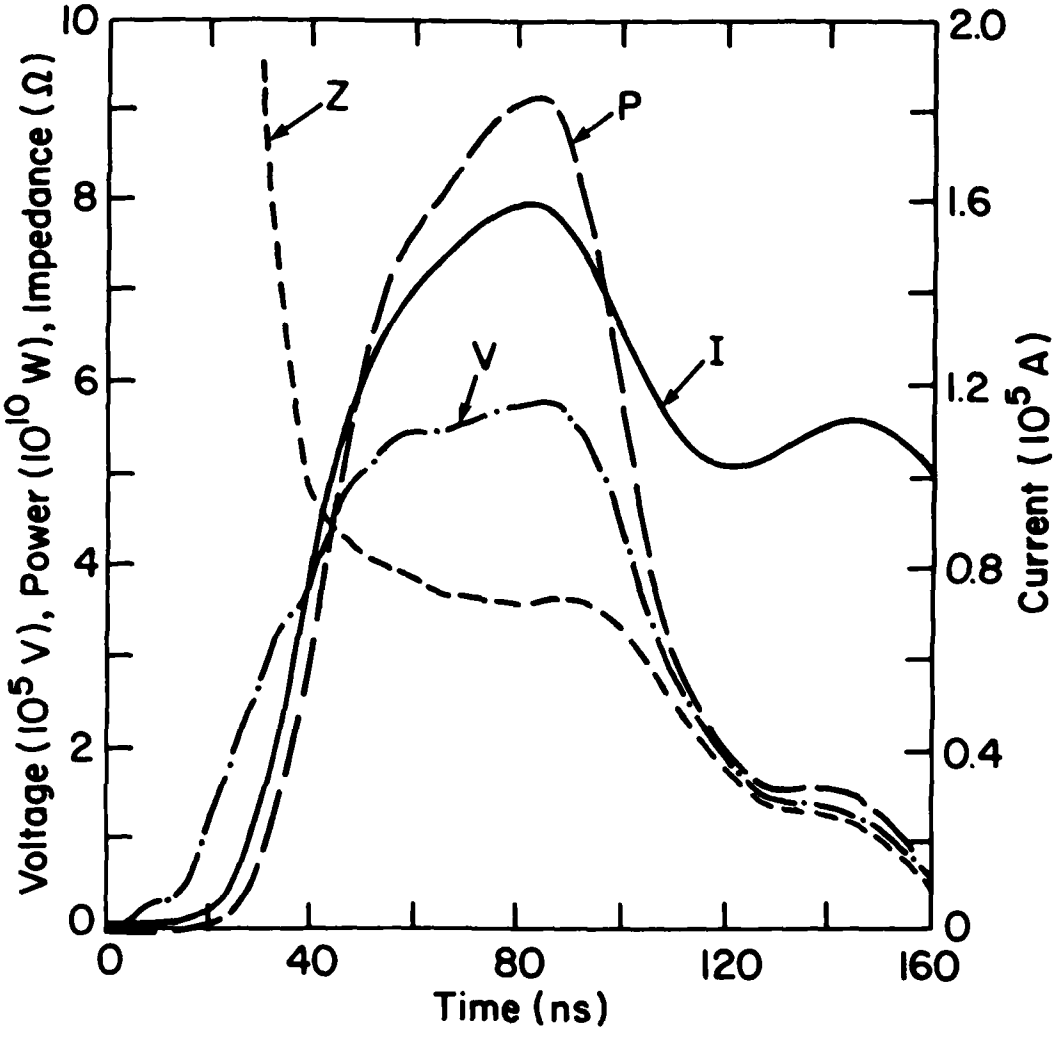

Figure 12 — Average overall diode parameter for shots #6442-6446

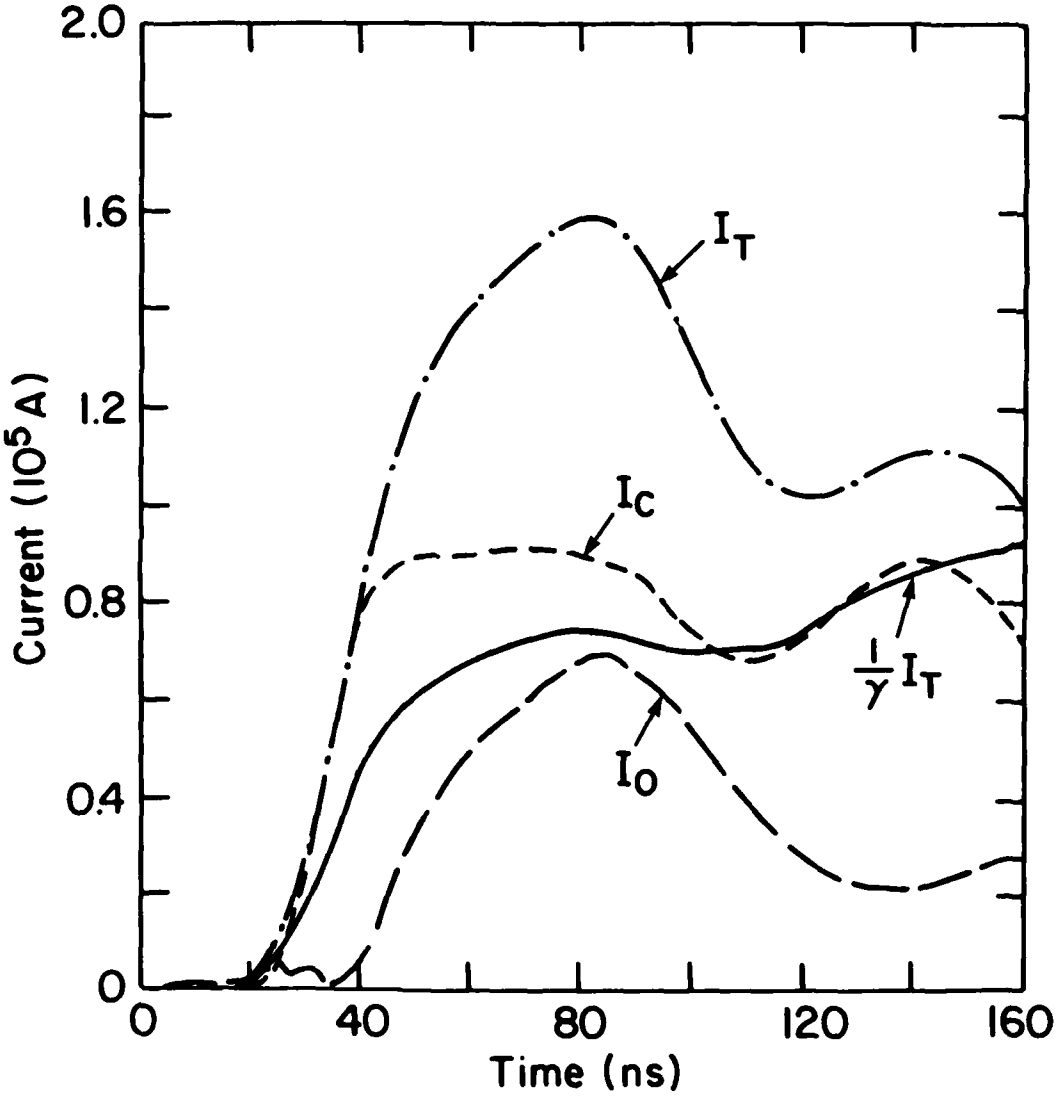

Figure 13 — Average Inner, Outer, Total, and Theoretical Bias Current for shots #6442-6446

D. CONCLUSIONS

A comparison of analytic theory, numerical simulation results, and experiments indicates that bias-current pinching via paravector-potential flow may indeed be realized. Detailed geometries of diodes specifically designed to allow a smooth transition from a PVP flow at large radii to an ion induced pinch flow at small radii were studied. With careful optimization, it may be possible to create very efficient electron pinches from large aspect ratio diodes.

It has been shown that the PVP diode concept allows the multiplication of the total current of a single, tapered, hollows cathode by a factor of γ_o without changing the geometry of the hollow cathode. In addition a fraction $(1\text{-}1/\gamma_o)$ of this current may be electron current independent of the diode aspect ratio or impedance. This contrasts with single, hollow cathodes which rely on ion induced pinching and contain a smaller fraction of their total current in electron current. The same diode may, however, operate with a bias current exceeding $\frac{1}{\gamma_o} I_l$ by allowing efficient ion production inside the center cathode. Preliminary results are encouraging and will be investigated further.

E. REFERENCES

1. Blaugrund, A. E. and Cooperstein, G., Phys Rev Lett *34*, 461 (1975).

2. Goldstein, Shyke A. and Lee, Roswell, Phys Rev Lett 35, 1979 (1975).

3. Blaugrund, A. E., Cooperstein, G. and Goldstein, S. A., Phys of Fluids *20*, 1185 (1977).

4. de Packh, D. and Ulrich, P. B., J. of Electronics and Control *10*, 139 (1961), and de Packh, D. Naval Research Laboratory, Radiation Project Internal Report No. 5, 1968 (unpublished).

5. Creedon, J. M., J. Appl. Phys *46*, 2946 (1975); and Phys Int'l Co. Report No. PIIR-17-72, 1972 (unpublished).

6. Friedlander, F., et al, Varian Associates Report No. DASA 2173, 1968 (unpublished).

7. Goldstein, S. A. et al, Phys Rev Lett *33*, 1471 (1974).

8. Poukey, J. W., in Proc of the Int'l Topical Conf. on Electron Beam Research and Technology, Albuquerque, New Mexico, 1975, edited by Gerald Yonas (U. S. Dept of Commerce, Washington, D.C., 1976), p. 247.

9. Stephanakis, S. J., et al, Phys Rev Lett. *37*, 1543 (1976).

10. de Packh, first experimental work on PPF cathodes on GI, (unpublished).

11. Yonas, G. et al, Phys Rev Lett. *30*, 164 (1973).

12. Read, Michael, PhD Thesis, Cornell University (1976).

13. Cooperstein, G. in NRL Memorandum Report No. 3006, p. 60 (1975); and G. Yonas (private communication).

14. Mendel, C. W. and Goldstein, Steven private communication.

15. Lee, Roswell, Goldstein, Shyke A. and Bacon, D. P. Bull. Am. Phys. Soc *23*, 762, (1978).

16. Quintenz, J. P., J. Appl. Phys. *49*, 4377 (1978).

17. Johnson, D. J., et al, J. Appl. Phys. *49*, 4634 (1978).

III. ELECTRON TRANSPORT EXPERIMENTS

A. INTRODUCTION

The propagation of relativistic electron beams in plasma channels has, in the last decade,[1-7] received considerable interest due to its applications for energy transfer and pellet fusion. A rough division of this effect may be made by characterizing the electron beam as hot or cold. In both cases, the relativistic electron beam propagates in a plasma having a self-consistent azimuthal magnetic field which confines the electrons radially. The necessary magnetic field for hot beam propagation (electrons injected with a large mean angle) is given by Alfvén's treatment of electron orbits which yields the condition that the net current inside the beam radius must be in the same direction as the beam current and nearly equal to the Alfvén current for the energy of the relativistic electrons.

$$I_{ch} \cong I_a = 17\,(\gamma^2 - 1)^{1/2}\,kA \tag{1}$$

On the other hand, for relatively cold beams (mean angle of injection $\theta << 1$), the same treatment indicates that the current needed is only

$$I_{ch} \cong (1 - \cos\theta)\, I_a \cong \frac{1}{2}\theta^2 I_a \tag{2}$$

In order to propagate 1 MeV electrons with a 10° mean injection angle, one needs only about 1 kA of net current in the channel compared to the 50 kA of net current needed for hot beam propagation. For typical beam currents of a few hundred kiloamperes injected into plasmas at densities of the order of 10^{18} cm^{-3}, the return current induced in the plasma is nearly equal to the primary beam current, leaving a net current of the order of 1% of the beam current. The remainder of the return current flows outside of the beam radius. The resulting net current of a few kiloamperes within the beam radius is sufficient to propagate relatively cool beams (as discussed above) but is insufficient for the propagation of a hot beam. Other means for providing the needed net current must therefore be utilized for hot beam propagation. Historically, these included z-pinch plasmas[5], and axial discharges via exploding wires.[6,7]

In the present work, the physics of the propagation of hot beams in plasma discharges driven by exploding wires is described. The work extends previous work[6,7] into a regime of higher beam currents (up to 300 kA injected) and investigates the effect of channel current and diode voltage on beam propagation. The effects of scattering and axial electric fields on electron orbits as well as the limitations on the maximum beam current and beam current density that can be propagated is investigated.

B. EXPERIMENTAL APPARATUS AND OBSERVATIONS

The experimental results of the present work were obtained on the GAMBLE I (800 kV, 220 kA, 80 ns FWHM) and GAMBLE II (1000 kV, 420 kA, 50 ns FWHM) electron beam facilities. A schematic of the experimental apparatus is shown in Fig. 1. An 84/39 mm (O.D./I.D.) hollow cathode with a 6° taper and 5.1 mm anode-cathode gap (at the inner diameter) was used. The anode was a 1.5 mm thick brass plate with a 20 mm diameter hole on axis. The hole was beveled at 30° on the cathode side and sanded to provide a smooth transition region for the radial electron flow. The hole was covered with a 25 μm titanium foil which was both ground plane and vacuum window. Immediately behind this was mounted a 20 μm aluminum foil to which a 51 μm tungsten wire was affixed. The wire was stretched in air from the center of the foil through the aluminum target plate, located 30 to 64 cm away, to a 56 μf, 2.4 μh (total circuit inductance), 20 kV capacitor bank. A "squirrel cage" of aluminum rods and rings served as a symmetric current return for the channel current. This bank could drive a peak current of 50-80 kA (occurring approximately 15 μs into the pulse) in an air plasma surrounding the wire.

The experimental diagnostics included diode voltage and current monitors, time integrated hard x-ray pinhole cameras looking at the anode, plasma channel, and target, open shutter

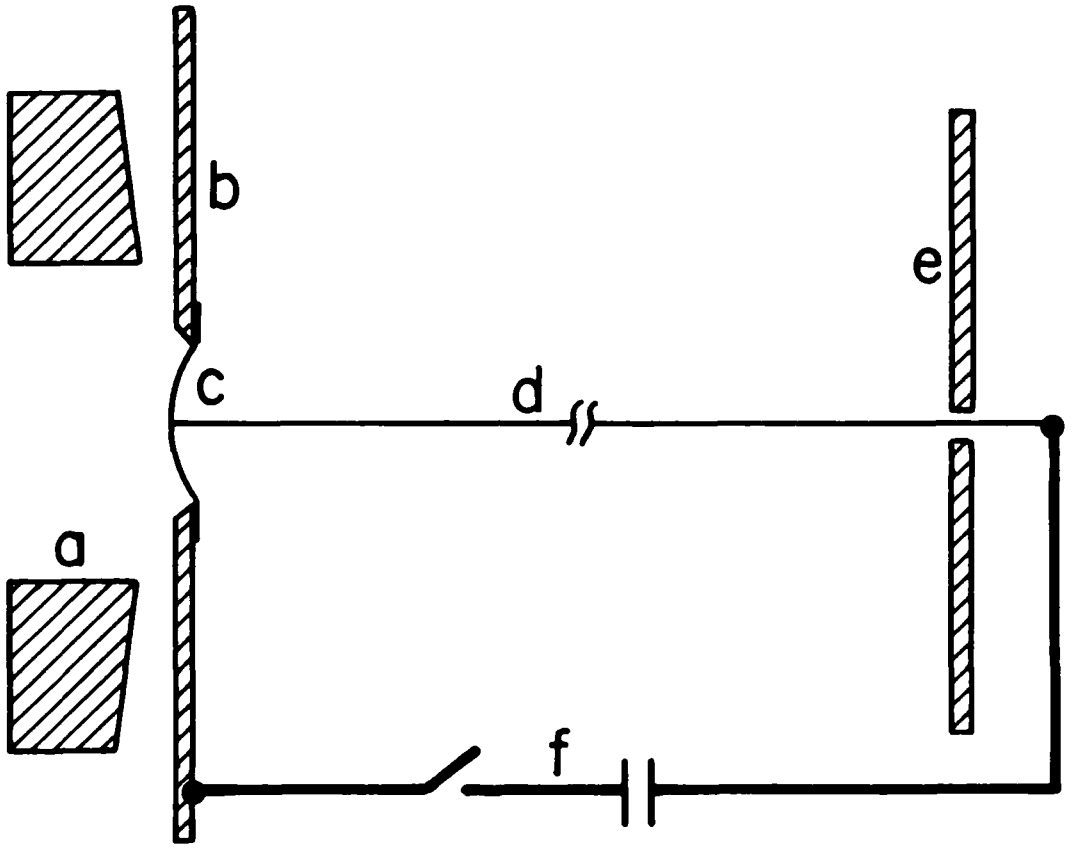

Figure 1 — A schematic of the experimental apparatus showing a) the brass cathode, b) the brass anode, c) the titanium/aluminum foil assembly, d) the tungsten wire, e) the aluminum target, and f) the switch and capacitor bank which supplies the channel current.

visual photography of the channel, time resolved, calibrated x-ray p-i-n diode detectors, and self-integration-B_θ and Rogowski coils monitoring the channel current. In addition, thermoluminescent detectors were used to obtain the peak energy of the transported electrons. Streak camera measurements of the plasma channel over the times of interest allowed one to determine the channel radius at the time of beam injection. This was verified by the time-integrated x-ray photographs of the channel. The channel's resistance was measured by the shift of the frequency of the ringing channel current from its zero resistance value — measured by replacing the wire with a 1.5 cm diameter conducting rod — and by the current decay time. Using an average channel radius ($r_{ch} \approx 1.6$ cm) allowed one to estimate the channel's conductivity to be $\sigma \approx 2 \times 10^{14}\ s^{-1}$, and temperature to be $T \approx 2$ eV. These parameters are consistent with theory.[8]

On GAMBLE I, the channel current was varied from about $\frac{1}{2} I_a$ to 2 I_a, while the anode hole (which limited the maximum injection radius) was varied from less than to greater than the channel radius. Propagation was successful only when the channel and beam currents had the same direction, in agreement with the theoretical prediction. In addition, it also became obvious that a crucial element of the experiment was the diode-channel interface. It was observed that any asymmetrical magnetic field at the target location caused a distortion in the electron distribution at the target. The inference to a similar effect at the diode-channel interface is made even more important as any current feed assymetry at the diode-channel interface could result in stray magnetic fields in the diode which could affect not only the beam injection, but also the diode physics.

Table 1 documents some important GAMBLE I shots. Shown are the diode voltage and current, the channel current and radius (determined from the beam injection time and the

plasma expansion velocity—about 0.8 cm/μs—and confirmed by x-ray and visual streak photography), the radius r_a which enclosed the Alfvén current, the radius of front surface damage r_D, and the radius of the back surface spall r_s.

Table 1 — Experimental Parameter Summary

Shot #	V(kV)	I(kA)	I_{ch}(kA)	r_{ch}(cm)	r_a(cm)	r_D(cm)	r_s(cm)
5693	700	230	80	1.6	1.1	1.1	—
5695	700	230	77	1.4	1.0	1.0	0.7
5700	800	220	68	1.6	1.2	1.2	0.9
5701	700	185	58	1.6	1.3	1.4	1.0
5903	510	205	42	1.4	1.2	1.2	0.8
5955	540	270	38	1.0	0.9	0.9	0.6

Figure 2 shows the diode voltage and current and the target x-rays for Shot 5700 on GAMBLE I. Thermoluminescent detectors allowed one to obtain an electron kinetic energy loss in the anode foil and plasma channel of 80 keV. Using this energy loss and the diode voltage gave the energy of the electrons striking the target. The collimated p-i-n detector looked at the central 3.5 mm radius of the target. From the electron energy and the p-i-n signal, a peak central current of 22 kA was calculated. Extrapolating the inferred current density out to the spall radius implied a propagated current of 145 kA. This is out of 195 kA of electron current in the diode (220 kA total diode current - 25 kA ion current computed using the Goldstein-Lee formula[9]) or a propagation efficiency of 74%.

On GAMBLE II, no parameter study was done. The goal was to propagate a high beam current density. On four shots, calibrated x-ray p-i-n detectors indicate that more than 200 kA

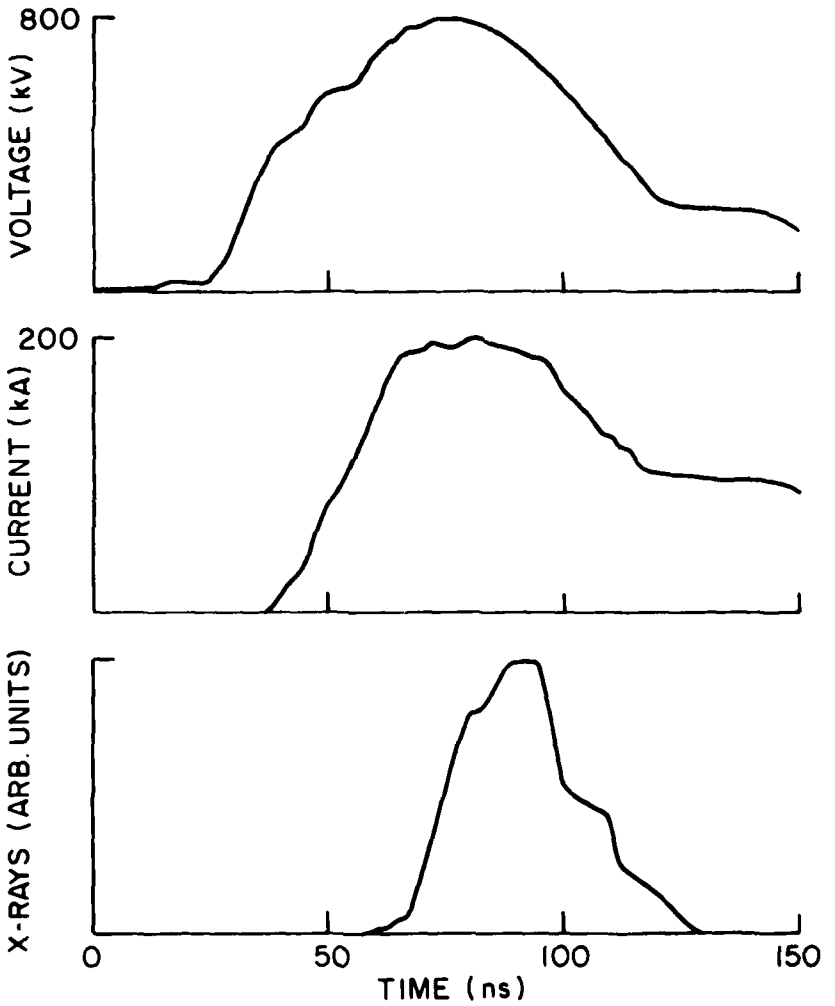

Figure 2 — Diode voltage, current, and x-ray pulses for GAMBLE I Shot 5700

of electrons propagated in the channel. In addition, a fifth shot is believed to have propagated more than 200 kA based on a comparison of target damage with known shots.

On GAMBLE II, the wire channel was independently viewed with another p-i-n detector. It indicated that less than 20 kA of electrons were lost in the plasma channel. This, however, is an upper limit as it assumed that the primary collisions occurred between the electrons and the low-Z plasma channel rather than the tungsten wire.

Figure 3 shows the diode voltage and current for GAMBLE II Shot 1799. In addition, the calibrated p-i-n signal is shown. Its peak signal corresponds to a current of approximately 160 kA. Since the p-i-n viewed only the center 5.3 mm radius, this indicated an average current density over this region of about 180 kA/cm^2. From the x-ray pinhole photograph, the area of the target x-rays (FWHM) was determined to be approximately 1.6 cm^2 and the total propagated current to be about 280 kA. This is out of a diode electron current of 330 kA (420 kA total diode current – 90 kA ion current) or an efficiency of approximately 85%. Two other shots gave propagation efficiencies over 50%, one of which had the p-i-n looking at the whole target plate and giving 255 kA.

Figures 4 and 5 show the x-ray pinhole photographs for the shots described above. At the top of Fig. 4 is a photograph taken with two different pinholes; the lower providing greater resolution. (Since the wire itself appeared as a line source, the size of its image provided a measure of the resolution.) On the left, electrons striking the edge of the hole in the brass anode produced the annulus surrounding the x-ray image of the pinched beam passing through the titanium anode foil. In the top image, the x-rays produced by electrons in the plasma channel can be seen. The target is not seen. At the bottom of Fig. 4 is a photograph taken with another pinhole camera which shows the entire system from left to right. Since the target was

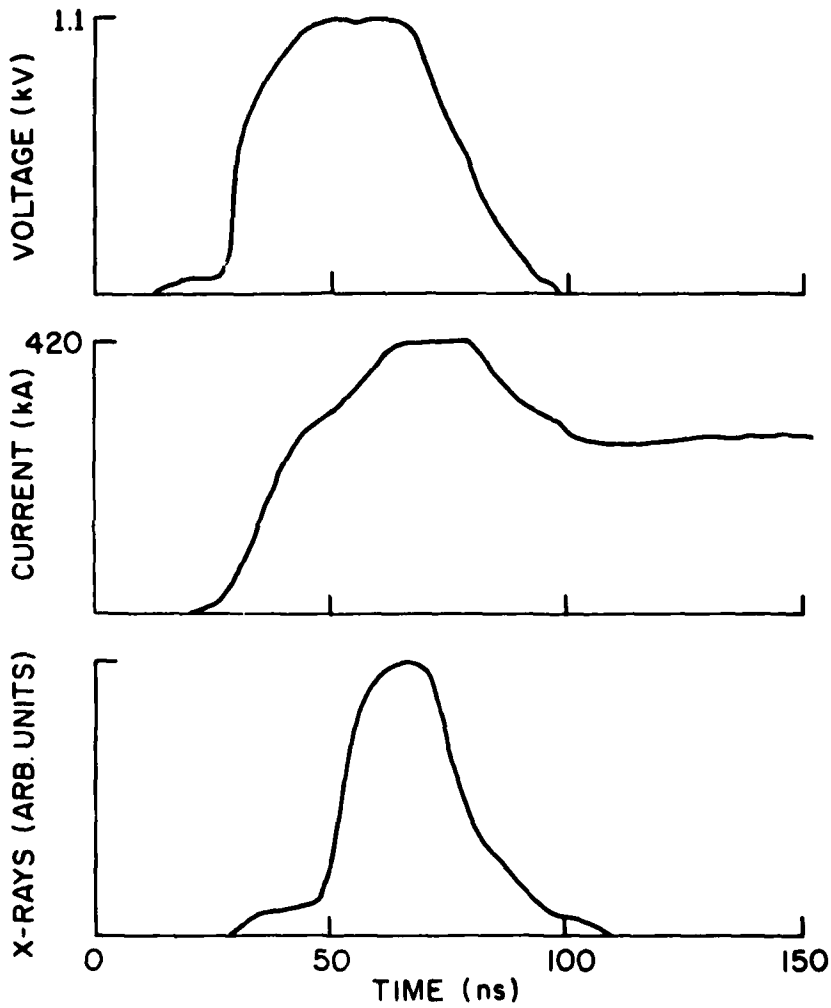

Figure 3 — Diode voltage, current, and x-ray for pulses GAMBLE II Shot 1799

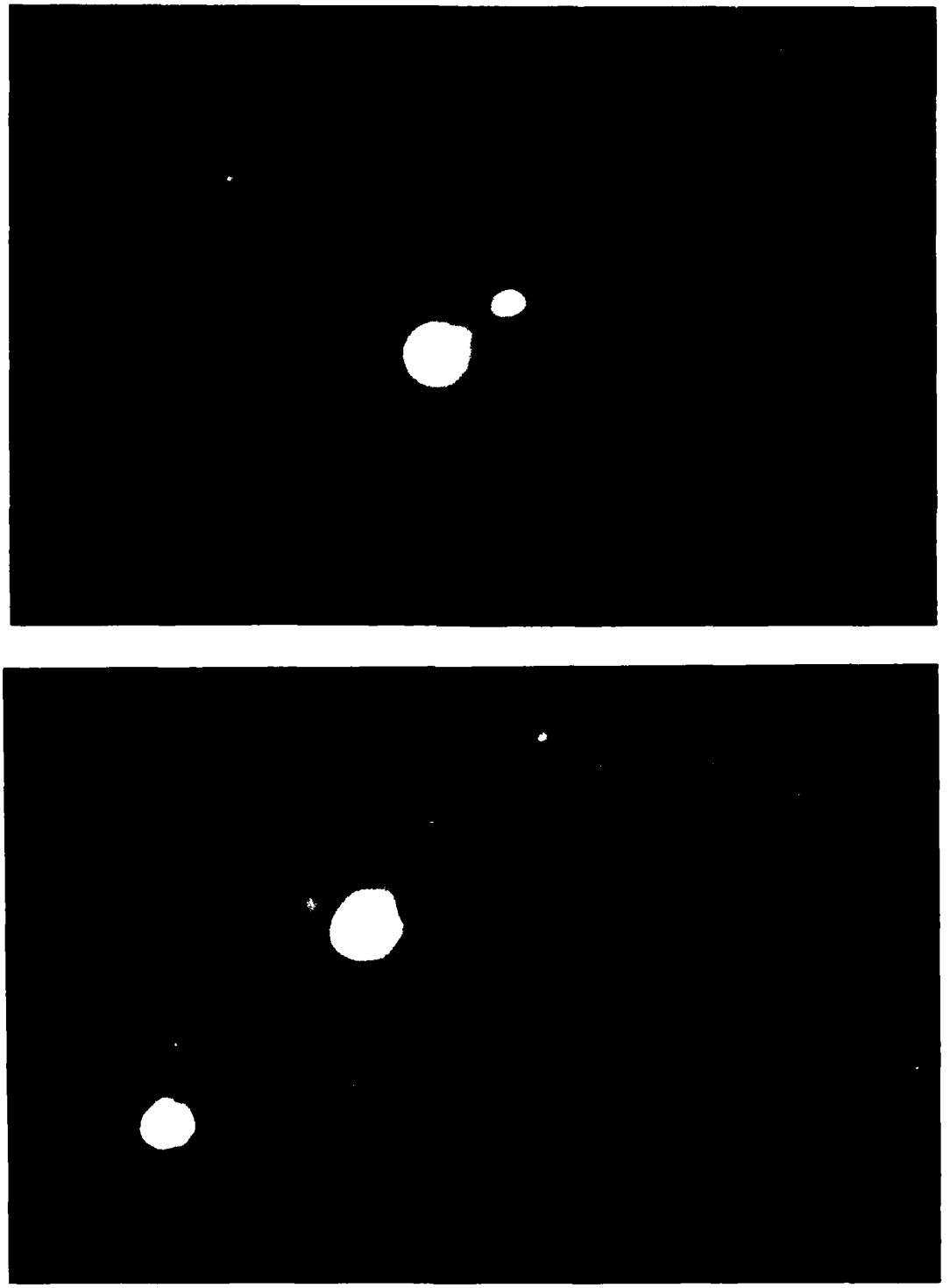

Figure 4 — X-ray pinhole photographs for GAMBLE I Shot 5700

Figure 5 — X-ray pinhole photograph for GAMBLE II Shot 1799

closer to the camera than the anode, the relative magnifications are different. On the left is the anode with the inner halo corresponding to an end-on view of the plasma channel. At the center of the anode is an image of the injected pinched beam while at right can be seen the image of the electrons as they strike the target. Figure 5 shows the propagation of electrons for GAMBLE II shot 1799. The circular ring around the target is pinhole shine-through while the crosshairs used for alignment are seen as an absence of exposure.

C. DISCUSSION

The problem of relativistic electron flow in plasmas heated before beam injection has been treated at length in the literature.[10] Most of the treatments were concerned with the plasma current response to the injected beam current. Two effects were neglected.

First, the conducting plasma has a finite radius outside of which there exists only low conductivity, cool air (theoretical models assumed high conductivity at all radii). The total return current is forced to run in the conducting plasma due to the voltage increase on the target for the relativistic electron beam. This differs from present theory which includes inductive effects only. The fact that the return current is forced to run in the plasma also explains why the B_θ loop placed outside the plasma (in both NRL and SLA experiments) showed essentially zero current change during beam transport. There may be about 0.1% of the primary beam current going through the capacitor bank and the return current rods connected to the anode plane of the generator[11] but this is too small a current to be detected with the B_θ loop in the present experiments.

Second, the hydrodynamics of the plasma has not received proper treatment. Usually, magnetic fields are viewed as confining fields perpendicular to their direction because of their

pressure tensor. In the case of beam injection into a conducting plasma, however, the magnetic field acts to confine the beam particles but at the same time the plasma is pushed outwards. The larger the magnetic field the greater is this expansion force. The reason for the reversal of the role of the magnetic field is that the return current set up in the plasma in response to the injected beam flows in the direction opposite to the beam current. This plasma current $j_p \simeq -j_b$ experiences a $j_p \times B_\theta$ force that causes plasma expansion. For constant beam current densities and for times shorter than magnetic diffusion times, the force causes constant acceleration with a radial expansion proportional to the time squared up to the beam pulse duration.

$$l_{\text{expansion}} \simeq \frac{j_p \times B_\theta}{2\rho c}\,\tau^2 \simeq 10^{-12}\,\frac{I_b I_{ch}\tau^2}{\pi r^3 \rho} \tag{3}$$

where the beam and channel currents (I_b, I_{ch}) are given in kA, beam pulse time in 10^{-8} s, plasma radius is assumed equal to beam radius and given in cm, and the plasma density ρ is given in g/cm^3. The expansion is less that 10^{-2} cm for the present and past[6,7] experiments because of large radii ($r \simeq 1$ cm) and low current ($\sim 10^5$ A). If however, 10^6 A would have been attempted with $r \approx 10^{-1}$ cm, the plasma would have expanded more than its initial radius during 50 ns and the current density would have dropped to the 10^5 A/cm^2 level.

It is thus concluded that the present experiments in open air were performed at high density with little hydrodynamic effect during the beam propagation while Physics International experiments[5] with tapered Z-pinches and low densities ($\rho \approx 10^{-7}$ g/cm^3) were strongly affected by hydrodynamic expansion.

Some limitations on current propagation are now considered. The simplest limit is that due to the plasma conductivity. An electric field $E = j_b/\sigma_p$ is needed to drive $j_p \simeq -j_b$. An upper limit on this field for one Gamble II experiment is 16 kV/m. The question of magnetic field diffusion and its effect on electron beam trajectories is now considered.

Because of finite channel conductivity, the magnetic field profile will change. The time scale for change over a length r in the radial direction is given by

$$\tau = \frac{4\pi\sigma r^2}{c^2}$$

For a length scale $r = 0.5$ cm and plasma conductivity of $\sigma = 2 \times 10^{14}\ s^{-1}$, $\tau = 750$ ns. The plasma temperature of 2 eV is obtained from heating by the discharge current during 20 μs. Little additional heating is expected for 10^5 A/cm^2 beam currents and the plasma densities in the experiment. During a 100 ns pulse, the net current will then increase by $\Delta I \approx 0.15\ I_b$, or 30 kA for $I_b = 200$ kA. The increased magnetic field due to the net current drastically affects the electron orbits. If the beam radius at injection is nearly equal to the plasma channel radius, the relativistic electron injected at large angles will be returned to the diode by this magnetic field and the efficiency of propagation will be reduced. If, however, the beam radius is initially smaller than the channel radius, then the electrons will expand radially to a radius smaller than the channel radius. As the net current increases, this radius will decrease and the beam will propagate at a higher current density. No reduction in efficiency will then be observed. This effect should be more pronounced at higher total beam currents. The experiments on Gamble I, Hydra and Gamble II are characterized by beam currents of 100, 200, and 250 kA respectively. In view of the above discussion, one should have observed the tightest pinches propagated on Gamble II. This was indeed observed.

The effect of time variation of diode voltage is important since a channel current nearly equal to I_α is needed for transport. When diode voltage is reduced the needed channel current is accordingly reduced. The combination of initial channel current and increase by magnetic diffusion brings the total current above I_α as diode voltage falls. This is one of the reasons why Gamble I or Hydra (which had nearly constant voltage pulses) show almost constant efficiency

of transport, while fast-changing impedance experiments on Gamble II showed a drastic reduction of beam transport efficiency during the 50 ns pulse.

Based on the preceding discussions, limits on the total current that can be transported using the present technique can now be determined. First, the conductivity defines an electric field which cannot exceed the diode voltage divided by the channel length. For $V = 1$ MV, $\sigma = 2 \times 10^{14}\ s^{-1}$ $l = 1$ m, the limiting current density is 2×10^6 A/cm^2. For a distance of 10 meters, only 2×10^5 A/cm^2 can be transported in these channels. At the higher current densities estimates will be modified by the higher temperatures and conductivities associated with beam and return-current heating.

Second, the plasma channel expansion limits the tightness of the transported beam. If the 2 MA/cm^2 beam of 1 MV electrons discussed above is injected into a 5 mm radius air channel carrying the Alfvén current, the channel radius will double in 50 ns. Even taking magnetic diffusion into account, the Alfvén radius will still be 1.2 times the original channel radius.

It has been shown experimentally that high-power-density electron beams may be efficiently transported using current-carrying air-plasma channels. It has been shown that certain restrictions apply to their use, the most restrictive being the limitation on the current density. This restriction may be overcome to a certain extent by increasing the channel temperature. This might be accomplished by using a lighter background gas. The self-consistent problem of plasma-channel expansion occurring simultaneously with the magnetic diffusion and its ultimate effect on the transported beam and the transport efficiency must still be studied.

D. REFERENCES

1. H. Alfven, Phys Rev *55*, 425 (1939).

2. D.A. Hammer and N. Rostoker, Phys Fluids *13*, 1831 (1970).

3. Roswell Lee and R.N. Sudan, Phys Fluids *14*, 1213 (1971).

4. L.S. Levine, et al, J. Appl Phys *42*, 1863 (1971).

5. J. Benford and B. Ecker, Phys Rev Let *26*, 1160 (1971); *28*, 10 (1972).

6. P.A. Miller, et al. Phys Rev Lett *39*, 92 (1977).

7. P.A. Miller, et al, in *Proceedings of the 2nd International Topical Conference on High Power Electron and Ion Beam Research and Technology* (edited by J.A. Nation and R.N. Sudan), 393 (1977).

8. A.F. Aleksandrov, et al, Zh. Ekop. Teor. Fig. *61*, 1841 (1972).

9. S.A. Goldstein and R. Lee, Phys Rev Lett *35*, 1079 (1975).

10. See Roswell Lee and R.N. Sudan, Physics of Fluids *14*, 1213 (1971) and the references contained therein.

11. Shyke A. Goldstein, et al, in *Proceedings of the 2nd International Topical Conference on High Power Electron and Ion Beam Research and Technology*, 71 (1977).

IV. REFLEXIVE FOCUSSING

Purely-ballistic focussing is not appropriate in a light-ion driven fusion reactor scenario where large focal distances are required. This is because of limits imposed by transverse ion motion brought about by finite anode temperature, scattering, or fluctuating diode fields. If these effects lead to a transverse-thermal-velocity spread in the beam characterized by V_{th}, then the minimum size to which the beam may be focussed can be approximated by

$$a \approx L\Delta\theta \tag{1}$$

where L is the focal distance from the diode to the target and $\Delta\theta$ is the beam divergences $\approx V_{th}/V_a$. Here, V_a is the axial ion velocity. Now, if a = 1 cm and $L = 10^3$ cm as required for a reactor, allowable values of $\Delta\theta$ are unrealistically small by one to two orders of magnitude. (Based on current knowledge, $\Delta\theta$ in the range of a few degrees appears reasonable.) One must then seek a magnetically-assisted focussing technique to provide the necessary standoff.

Magnetic-focussing techniques have been discussed in the literature. However, neither technique is appropriate for the delivery of MA/cm^2 ion beams to distant targets. Both involve the use of large applied magnetic beams to distant targets. Both involve the use of large applied magnetic fields in the diode and are therefore appropriate to a reflex-triode mode of ion beam production. The low ion-current-density capability of this technique coupled with an upper limit of an order-of-magnitude increase in ion-current density associated with the two focussing schemes leads to to deliverable ion-current-densities which are too low to meet pellet requirements. Although self-pinch diodes can produce the required current density, the applied field must be excluded from the diode for the ion production mechanism to operate. In that case, the large angular velocity induced as the emerging beam enters the field-filled region then prevents focussing. Additionally, both focussing techniques employ curved magnetic-field lines

which induce currents in the propagating charge-neutral beam. In order that these currents not disrupt the focus, the energy-density of the beam cannot exceed that of the applied fluid; a condition which cannot be satisfied in the vicinity of the focus.

For the problem at hand, it may be desirable to carry out focussing with standoff by employing weak guide fields with straight lines of force. This can be accomplished by introducing the beam at a small angle to the field and allowing the large gyro-radius motion of the ions to bring the beam to focus meters downstream. Since the ions must move across the magnetic field, charge and current neutralization cannot be provided by electrons extracted from the diode. A background plasma or gas fill is therefore required. The reflexive-focussing technique just described is shown schematically in Fig. 1. The anode is curved so that the beam is made to diverge. The symmetry of the single-particle motion about the midplane causes the real focus on the right-hand-side of the figure to reflect the virtual focus to the left to the diode. Thus, although transported over a long distance L, the final focus is characterized by the shorter length z_f. For this reason, thermal beam spreading does not severely limit focusability since L is replaced by z_f in Eq. (1). The remainder of this section is devoted to a kinetic-theory analysis of this concept.

It is assumed that complete charge and current neutralization exists so that the ions move only in the applied solenoidal field. The beam-ion distribution function therefore satisfies

$$v_r \frac{\partial f}{\partial r} + v_z \frac{\partial f}{\partial z} + \left(\frac{v_\theta}{r} + \Omega \right) \left(v_\theta \frac{\partial f}{\partial v_r} - v_r \frac{\partial f}{\partial v_\theta} \right) = 0 \tag{2}$$

where $\Omega = eB/m_i$ is the ion gyrofrequency. Forms for f which depend only on the single-particle constants of the motion satisfy this equation, i.e.

$$f = f(E, V_\theta, p_\theta, U) \tag{3}$$

REFLEXIVE FOCUSING

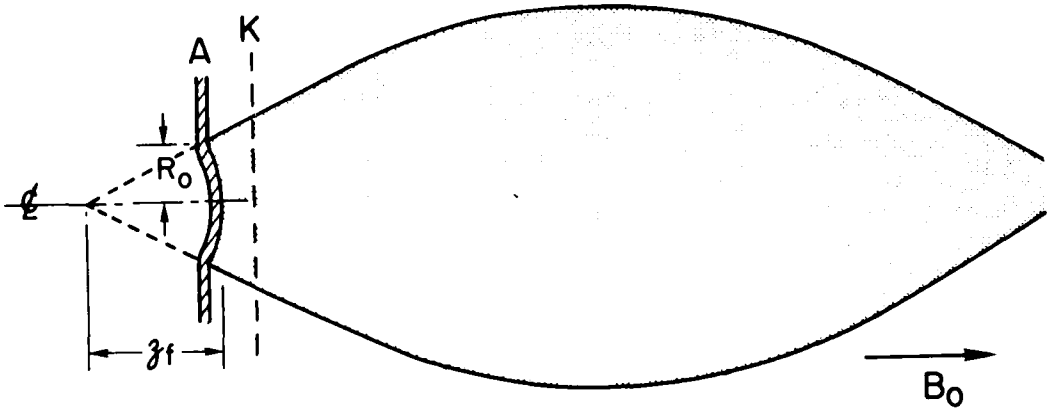

Figure 1

where

$$V = v_z;\ E = v^2 - v_z^2;\ p = rv_\theta + \tfrac{1}{2}\Omega r^2;$$
$$U = \Omega r v_r \cos\zeta - (v_r^2 + v_\theta^2 + r\Omega v_\theta)(\sin\zeta - \sin\phi) + \tfrac{1}{2}\Omega^2 r^2 \sin\phi \tag{4}$$

and $\zeta = \Omega z/v_z + \phi$. The quantity ϕ is a constant.

The desired solution must satisfy a number of requirements. The distribution function must reflect the radial divergence of the beam at injection. The beam must be allowed to have rigid rotation within certain limits at injection since all, or any fraction of, of the solenoidal field may be allowed to penetrate the diode region. Since the beam is born with zero angular momentum, the beam emerging into the drift section will have an angular velocity (given by conservation of p) of

$$v_\theta(z) = (\Omega - \Omega_i)r = \omega r$$

where Ω_i is the ion gyrofrequency associated with the solenoidal field in the diode. Thus, $-\Omega/2 \leqslant \omega \leqslant 0$ for positive Ω. The beam radius must be finite (characterized by radius R at injection) and a transverse thermal velocity spread is desired. Finally, the distribution function must be analytically tractable. An appropriate form for f is

$$f = \frac{n_i}{\pi L^2}\, H(L^2 - U^2)\delta(V - V_i)\exp\left(\frac{AE + Bp + CU}{L^2}\right) \tag{5}$$

where $H(x) = 1$ for $x \leqslant 0$ and zero otherwise. The quantity L therefore specifies the beam radius at injection into the drift space ($z = 0$), and n_i is the axial beam-ion density there.

Although satisfying all of the above requirements, Eq. (5) relaxes exact energy conservation for all ions since $V = v_z$ cannot be constant as a function of t when transverse velocity components exist. Consideration is therefore limited here to cases where $L^2 \gg E$, i.e. cases for which the transverse energy content of the beam is small.

The constants A, B, C, and ϕ are chosen to reflect the desired velocity distribution at $z = 0$.

$$AE + Bp + CU(z = 0) = (v_r + rV_o/z_f)^2 + (v_\theta - \omega r)^2 \tag{6}$$

For an initially diverging beam, z_f is negative. Equation (6) requires that

$$\tan \phi = \sigma + \frac{1}{\sigma} \frac{\omega}{\Omega} \left[1 + \frac{\omega}{\Omega}\right] \tag{7}$$

where $\sigma = V_o/\Omega z_f$. The small-transverse-energy constraint requires that consideration be limited to beams injected at small angles to the guide field, i.e.

$$|z_f| >> R \; ; \; \Omega R << V_o$$

for the radial and azimuthal velocity components.

The radial-density distribution at $z = 0$ can now be determined by integrating f over velocity space. This exercise results in the expression

$$n(r,0) = \tfrac{1}{2} n_o \left[\text{erf}\left[\Delta \frac{R^2 - r^2}{Rr}\right] + \text{erf}\left[\Delta \frac{R^2 + r^2}{Rr}\right]\right] \tag{8}$$

where

$$\Delta = \tfrac{1}{2} \sigma \delta \left[1 - \frac{1}{\sigma^2} \frac{\omega}{\Omega} \left[1 + \frac{\omega}{\Omega}\right]\right]$$

and $\delta = R\Omega/V_{in}$. Density profiles for various values of Δ are shown in Fig. (2). For the "cool" beams of interest here ($V_o >> V_{in}$), the beam profile is nearly square.

The average beam area as a function of axial position can be determined by integrating f evaluated along the axis of symmetry. This calculation yields

$$\frac{n(0,z)}{n_o} = \frac{1}{a(\zeta)} \left[1 - \exp\left[-\frac{\gamma a}{1 - a}\right]\right] \tag{9}$$

where

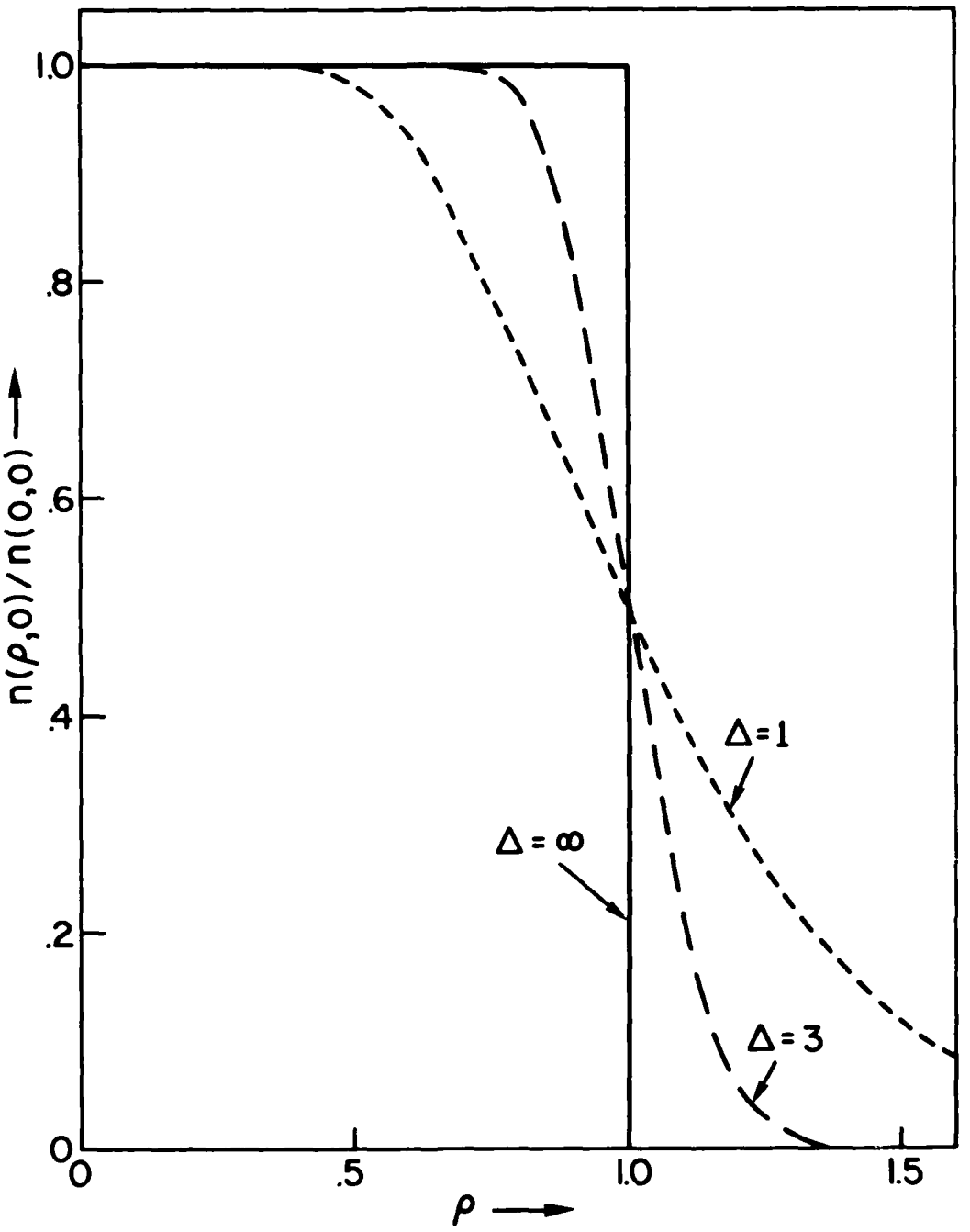

Figure 2

$$\gamma = \delta^2\sigma^2\left[1 - \frac{1}{\sigma^2}\frac{\omega}{\Omega}\left[1 + \frac{\omega}{\Omega}\right]\right] = 2\delta\sigma\Delta \tag{10}$$

and

$$a(\zeta) = 1 - 2\left[\sigma^2 + \frac{\omega}{\Omega}\left[1 + \frac{\omega}{\Omega}\right]\right]\left[\frac{\sin\zeta}{\sin\phi} - 1\right]. \tag{11}$$

Equations (9)-(11) show that for an initially diverging beam, $n(0,z)$ first decreases from n_o and then increase as the beam approaches a focus. The focus location L, the value of z for maximum density occurs very close to the point where a is minimum. From Eq. (11), minimum a occurs at $\zeta = \zeta_c$ where

$$\zeta_c = \Omega L/V_o + \phi = \frac{3\pi}{2} \tag{12}$$

with ϕ determined from the value of σ and Eq. (7). The radial beam density distribution at $\zeta = \zeta_c$ can again be determined by integration of f over velocity space with the result

$$\frac{n(r,L)}{n_o} = A\exp\left[-A\frac{r^2}{R^2}\right] \tag{13}$$

where

$$A = \frac{n(o,L)}{n_o} \tag{14}$$

is obtained from Eq. (9) with $\zeta = \zeta_c$. The quantity A is a measure of the degree of current-density multiplication occuring at the best focus. The variation of A with the thermal parameter δ is shown in Fig. 3 for various values of σ and the two limiting rotational frequencies. Best focussing is associated with $\omega = -\frac{1}{2}\Omega$ since this case corresponds to zero canonical angular momentum. For this choice, the minimum value of $a(\zeta)$ is zero so that A may be obtained from Eq. (9) in the limit of a going to zero.

$$A\left[\omega = -\frac{\Omega}{2}\right] = \gamma = \left[\frac{R}{z_f}\right]^2\left[\frac{V_o}{V_m}\right]\left[1 + \frac{\sigma^2}{4}\right] \tag{15}$$

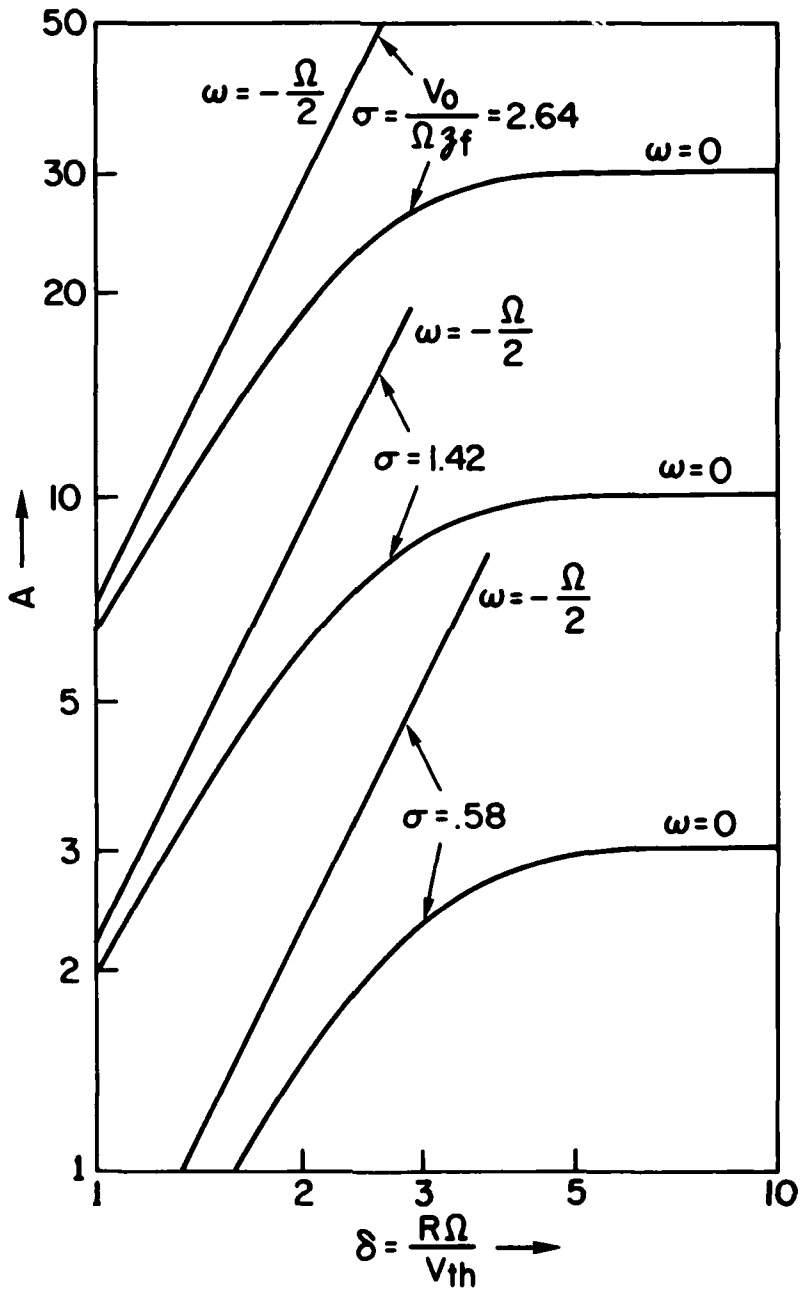
50
30
20
10
5
3
2
1
A
1
2
3
5
10
$\omega = -\frac{\Omega}{2}$
$\sigma = \frac{V_0}{\Omega \mathcal{J}_f} = 2.64$
$\omega = 0$
$\omega = -\frac{\Omega}{2}$
$\sigma = 1.42$
$\omega = 0$
$\omega = -\frac{\Omega}{2}$
$\sigma = .58$
$\omega = 0$
$\delta = \frac{R\Omega}{V_{th}}$

Figure 3

As suggested earlier, this is the same degree of focussing one would obtain ballistically using the focal length z_f rather than L in Eq. (1).

As an example of how reflexive focussing can be employed in a pellet-fusion reactor, consider a 10 MA beam of 10 MeV protons focussed onto a pellet of 1 cm^2 cross-sectional area 5×10^2 cm away from the diode. The required degree of focussing is $A = \pi R^2$ where R is the ion-emitting radius of the anode. Assuming that the major contribution to V_{th} arises from fluctuating fields in the diode leading to an about $\pm 1°$ time-dependent deflection of the beam-emission angle, then $V_o/V_{th} \approx 60$ so that Eq. (15) requires $z \approx 30$ cm. Simultaneous solution of Eqs. (7) and (12) leads to $\Omega L/V_o \approx 5$ so that the required solenoidal field is about 5 kG. Choosing $R \approx 5$ cm in order to satisfy the small-transverse-velocity requirement $|z_f| >> R$ leads to a diode aspect ratio of 15 for a 3 mm diode spacing. This ratio is well matched to the generator required to generat the 1 Ω ion beam.

V. MHD RESPONSE OF TRANSPORT CHANNELS

A. INTRODUCTION

With recent advances in the technology of intense light-ion beam generators,[1,2] the suggestion that these ion beam could be used in a pellet fusion scheme has drawn considerable interest[3] as have similar concepts using heavy ion beams[4] (e.g. 20 GeV U^+ ions). In a functioning reactor, the ion beam would have to be propagated a distance L (about 10 m) from the acceleration region while employing some focussing scheme to deliver the beam to the target.

For heavy ion beams, field-free ballistic focussing to the target has been proposed.[4,5] For light ion beams (e.g. 10 MeV protons), one concept[6] that is under investigation involves focussing the beam just outside the diode region by known techniques[1] and then injecting the focussed beam into a z-pinch plasma channel. The beam remains focussed during propagation by the magnetic field in the plasma channel and is delivered on target with no additional focussing. For both of these techniques, it must be demonstrated that the self-consistant electromagnetic fields associated with the plasma response to beam passage do not disrupt transport and focussing. We have started to investigate this problem by concentrating on the physics occurring in the plasma channel as a result of the ion beam passage. This area of investigation has been largely ignored in studies so far; it has been generally assumed that the channel does not respond to the beam on the time scale involved. With beam pulse lengths of 50 ns for light ion beams and of around 10 ns or more for heavy ion beams, this assumption is not generally correct for transport in channels of cm radius or less. Magnetic nonneutralization effects are important for large radius beams as well, since small (i.e. $\sim$ 1 kA) net currents are sufficient to destroy focussibility to mm spot sizes for heavy ion beams which are ballistically focussed.

Recent work has concentrated on the plasma response to light-ion beams with a view to answering the questions:

(a) Does a plasma-parameter window exist which allows efficient transport over 10 meter distances?

(b) Do the self-consistent electromagnetic fields associated with beam heating, net current effects and plasma hydrodynamics disrupt beam transport or its ability to bunch?

Some constraints which have to be satisfied by the beam plasma system include:

(a) The density in the hole bored by the applied z-discharge and beam currents must be sufficiently high to permit complete charge-neutralization.

(b) The beam-heated plasma must be sufficiently high in temperature to provide good magnetic neutralization.

(c) The temperature must be sufficiently high to reduce return-current electric fields to a level which neither slows the beam appreciably nor disrupts bunching.

B. SUMMARY OF CODE RESULTS

A 1-D radial, time-dependent, Eulerian code has been developed recently to answer these questions. The code solves the plasma moment equations, Maxwell equations, and transport equations using coefficients for electrical and thermal conduction taken from Braginskii.[7] The beam is specified by its current density in space and time. Direct beam energy deposition and radiation cooling as well as return-current heating have been included in the code. Initial conditions consist of a plasma z-discharge in a high-density gas.[8] The density of the discharge

channel is typically .01-.1 atmosphere of low-z gas while the background density may be much higher.

Preliminary results appear in Fig. 1. They correspond to a 1 MA, 10 MeV proton beam, 0.6 cm in radius propagating in a preformed hydrogen channel of the same dimension with an initial density on the axis of 2×10^{18}. Results shown are radial profiles for density, azimuthal-magnetic and axial-electric fields, and temperature at $t = 40$ ns into the beam pulse. These are the conditions which develop near the tail of the beam. No impurities have been included in this calculation so that only hydrogen bremsstrahlung losses are included. Time histories through any point fixed in the chamber of the maximum B-field, maximum temperature, central electric-field strength and minimum channel density appear in Fig. 2.

Conclusions which can be drawn at this point are:

(a) Hydrogen backgrounds of $1\text{-}3 \times 10^{18}\text{cm}^{-3}$ allow propagation satisfying all constraints to transport and bunching.

(b) Hydrodynamic expansion at lower densities may result in insufficient neutralizing densities.

(c) Low plasma temperatures at higher densities cause excessive return-current electric field strengths which slow the beam and perturb bunching. Line radiation from impurities in the background may also cause low temperatures to develop if present in sufficient densities.

Phenomena which have not been included in the code yet and which are important to a more complete understanding of the channel physics are:

- Non-equilibrium ionization of the plasma at the head of the beam.

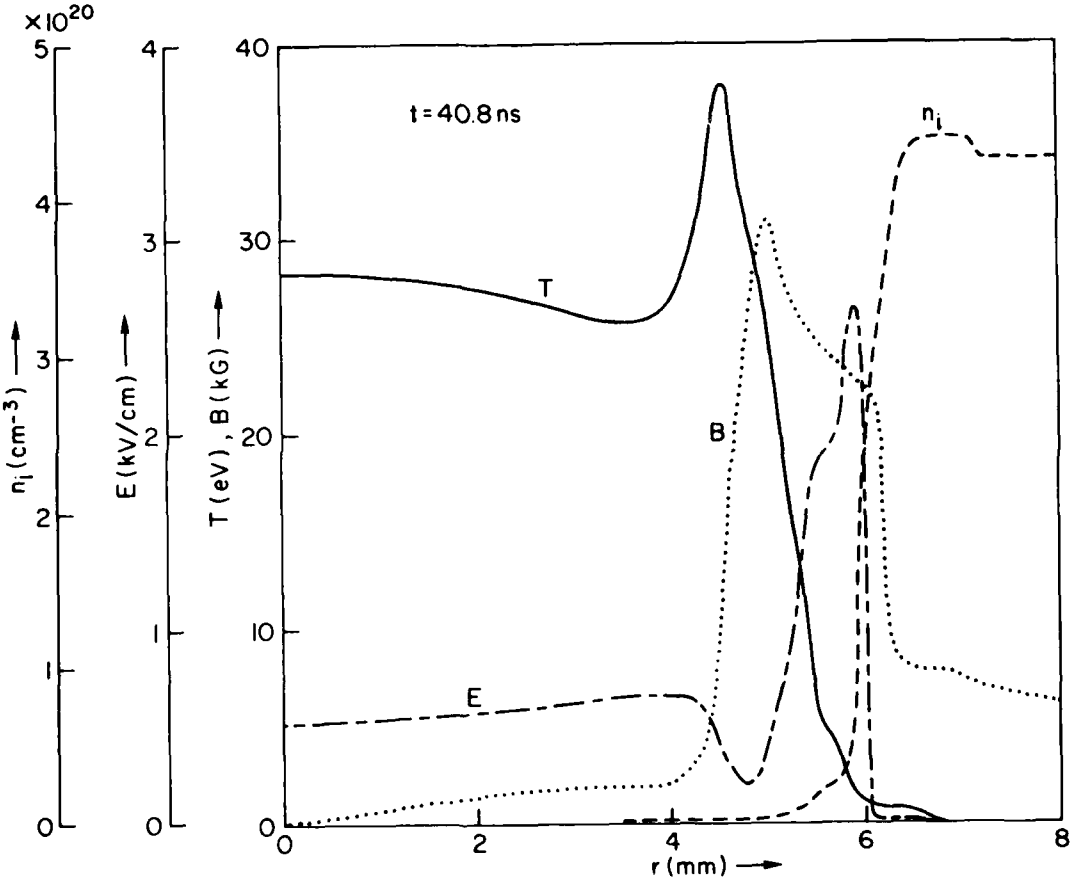

Figure 1

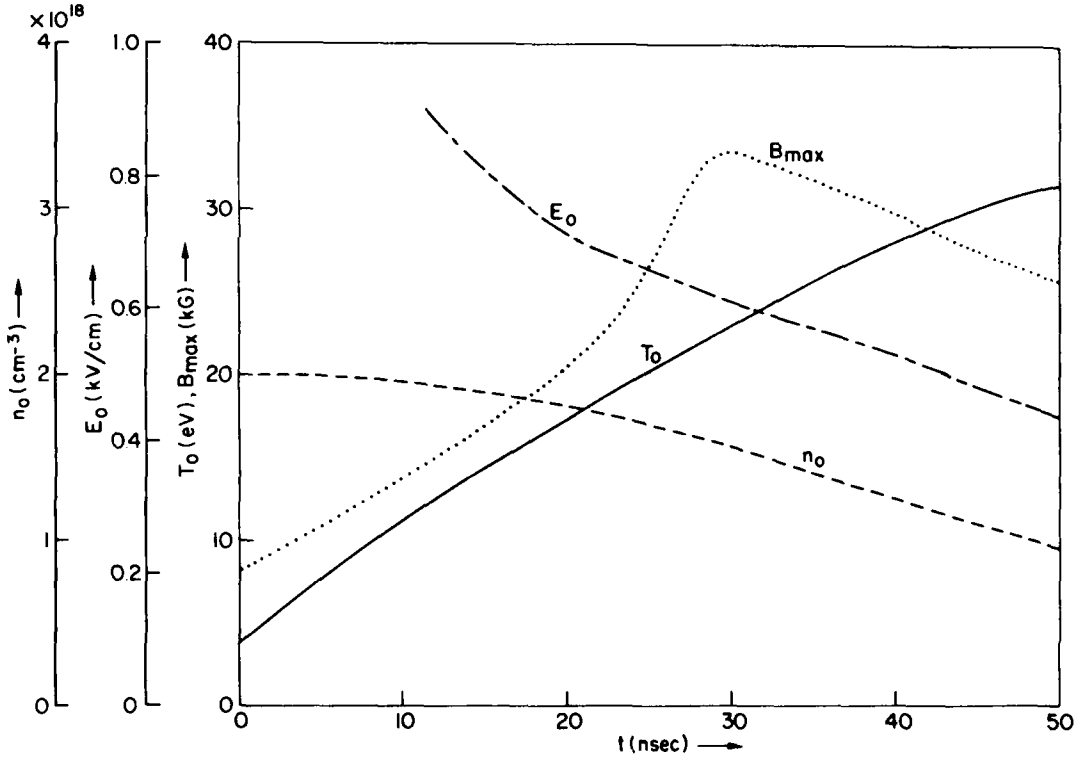
×10^18
4
3
2
1
0
n0 (cm-3)
1.0
0.8
0.6
0.4
0.2
0
E0 (kV/cm)
40
30
20
10
0
T0 (eV), Bmax (kG)
Bmax
E0
T0
n0
0
10
20
30
40
50
t (nsec)

Figure 2

- Values for electrical conductivity at low temperature which determines the penetration of the B-field into the plasma and the degree of current non-neutralization achieved late on in the pulse.

These phenomena plus comparison with experiments at lower current intensities (with correspondingly lower temperatures and ionization levels), extension of this work to heavy ion beams, and a more consistent treatment of the ion-current distribution in position and time due to self fields and bunching will constitute future developments of this work.

C. REFERENCES

1. D. Mosher, G. Cooperstein, S.J. Stephanakis, Shyke A. Goldstein, D.G. Colombant and Roswell Lee, presented at the 2nd International Topical Conference on High Power Electron and Ion Beam Research and Technology, Cornell University, Ithaca, New York (1977).

2. S.J. Stephanakis, D. Mosher, G. Cooperstein, J.R. Boller, J. Golden and S.A. Goldstein, Phys. Rev. Lett. **37**, 1543 (1976).

3. M.J. Clauser, Phys. Rev. Lett. **34**, 570 (1975).

4. A.W. Maschke, IEEE Trans. Nucl. Sci. **22**, 1825 (1975).

5. R.L. Martin and R.C. Arnold in Proceedings of the Conference on Heavy Ion Acceleration and Storage Rings for Pellet Fusion Reactors, Argonne National Laboratory, Argonne, Illinois (1976).

6. D. Mosher, Shyke A. Goldstein, P.F. Ottinger and W.W. Hsing, presented at the Topical

Meeting on Inertial Confinement Fusion, San Diego, California (1978).

7. S.I. Braginskii

8. S.A. Goldstein, D.P. Bacon, D. Mosher and G. Cooperstein, Proceedings 2nd International Topical Conference on High Power Electron and Ion Research and Technology, Cornell Univ., Ithaca, N.Y. (1977), p. 71.

9. P.J. Ottinger and D. Mosher, in Proceedings of the Heavy Ion Fusion Workshop, Brookhaven National Laboratory, Upton, New York (1977).

10. P.F. Ottinger, D. Mosher and S.A. Goldstein, NRL Memorandum Report 3784 (1978); to be published in Phys. of Fluids.

VI. SUPPORTING PUBLICATIONS AND REPORTS

The following papers taken together with the body of this report document DOE supported FY 77-78 research carried out in the NRL charged-particle-beam ICF program.

A. "Time-Dependent Impedance Behavior of Low-Impedance REB Diodes During Self-Pinching," by D.J. Johnson, Shyke A. Goldstein, Roswell Lee and W.F. Oliphant, J. Appl. Phys. **49**, 4634 (1978).

B. "Anode Scattering Effects on Electron Pinch Radius in Low-Impedance REB Diodes," by D.J. Johnson and Shyke A. Goldstein, J. Appl. Phys. **48**, 2280 (1977).

C. "Spatially Resolved EUV Emission from Focused REB Discharges into Thin Targets," by D.J. Johnson, W.F. Oliphant, G.A. Doscheck, and U. Feldman, J. Appl. Phys. **49**, 113 (1978).

D. "Magnetic Compression of Charged-Neutralized Ion Beams," by D. Mosher, Phys. Fluids **20**, 1148 (1977).

E. "Transport and Focusing of Intense Electron and Ion Beams Using External Magnetic Fields and Plasma Channels," by Shyke A. Goldstein, D.P. Bacon, D. Mosher and G. Cooperstein, Proc. High Power Electron and Ion Beam Research and Technology, Cornell U., Oct. 3-5, 1977.

F. "Microstability of a Focused Ion Beam Propagating through a Z-Pinch Plasma," by P.F. Ottinger, D. Mosher and Shyke A. Goldstein, Phys. Fluids **22**, 332 (1979).

G. "Experimental Investigation of Intense Ion Beam Transport," by F. Sandel, JAYCOR Memorandum Rep. 320-79-004-MR, 1978.

H. "Current Neutralization in Beams Traversing Gas Backgrounds," by D. Mosher, Proc. ERDA Summer Study of Heavy Ions for Inertial Fusion, Berkeley, CA, July 1976. Lawrence Berkeley Lab. Rep. LBL-5543, 1976.

I. "Current Neutralization of Converging Ion Beams," by D. Mosher, Proc. Heavy Ion Fusion Workshop, Upton, N.Y., Oct. 1977. Brookhaven National Lab. Rep. BNL 50769, 1978.

J. "Linear Microstability Analysis of a Heavy Ion Beam-Plasma System," P.F. Ottinger and D. Mosher, Ibid.

K. "Ion-Stopping Power of Ionized Media," by D. Mosher, Proc. ERDA Summer Study of Heavy Ions for Inertial Fusion, Berkeley, CA, July 1976. Lawrence Berkeley Lab. Rep. LBL-5543, 1976.

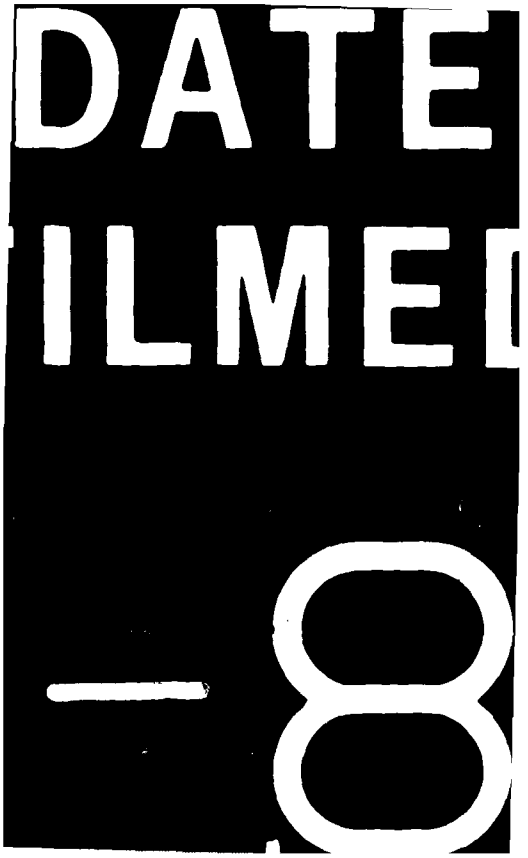
DATE
ILME
-8